AEDC-TR-73-154

# STUDY OF MOIRÉ MEASURING TECHNIQUES FOR WIND TUNNEL MODEL DEFORMATION

Manlio Abele, Charles Ruger, and Ernest Sanlorenzo
General Applied Science Laboratories, Inc.

September 1973



ARNOLD ENGINEERING DEVELOPMENT CENTER
AIR FORCE SYSTEMS COMMAND
ARNOLD AIR FORCE STATION, TENNESSEE

# NOTICES

When U. S. Government drawings specifications, or other data are used for any purpose other than a definitely related Government procurement operation, the Government thereby incurs no responsibility nor any obligation whatsoever, and the fact that the Government may have formulated, furnished, or in any way supplied the said drawings, specifications, or other data, is not to be regarded by implication or otherwise, or in any manner licensing the holder or any other person or corporation, or conveying any rights or permission to manufacture, use, or sell any patented invention that may in any way be related thereto.

Qualified users may obtain copies of this report from the Defense Documentation Center.

References to named commercial products in this report are not to be considered in any sense as an endorsement of the product by the United States Air Force or the Government.

# STUDY OF MOIRÉ MEASURING TECHNIQUES FOR WIND TUNNEL MODEL DEFORMATION

Manlio Abele, Charles Ruger, and Ernest Sanlorenzo
General Applied Science Laboratories, Inc.

# FOREWORD

This report describes the work performed on Air Force contract 40600-72-C-0009 by General Applied Science Corporation, Westbury, Long Island, New York.

The work was administered by the Department of the Air Force, Headquarters Arnold Engineering Development Center (TMP). Mr. Marshall K. Kingery, AEDC (DEL), is the technical representative.

This program was managed by Mr. Ernest Sanlorenzo of General Applied Science Laboratories.

The reproducibles used in the reproduction of this report were supplied by the author.

This technical report has been reviewed and is approved.

MARSHALL K. KINGERY
Facility Development Division
Directorate of Civil Engineering

ROLAND R. GARREN
Colonel, USAF
Director of Civil Engineering

## ABSTRACT

An analytical and experimental study has been conducted to determine the feasibility of using Moiré techniques for the accurate measurement of model distortions expected to be encountered in the HIRT Facility. A comprehensive study of the basic characteristics of Moiré techniques has been carried out to determine the best approach which could both satisfy the constraints imposed by the size and configuration of the test section, and provide the necessary accuracy in the measurement of the local distortion. The results of the study suggest the selection of a measuring technique where the grating is an integral part of the surface of the test model. A Moiré is formed by the superimposition of two images of the grating obtained in the undistorted and distorted condition of the test model. A null method of analyzing the Moiré pattern allows the accurate measurement of the local distortion. The report is presented in three parts. Part I presents a technical discussion of the measuring techniques as well as the experimental data obtained in a laboratory arrangement which simulates the anticipated test conditions. Part II discusses the implementation aspects of the recommended measuring technique. Part III contains the summary of various implementations of the Moiré principle and the recommendations regarding the selection of the most appropriate measuring technique.

# TABLE OF CONTENTS

# LIST OF ILLUSTRATIONS

# PART I

# DEFORMATION MEASUREMENTS BASED ON MOIRÉ TECHNIQUES

## 1. INTRODUCTION

The Moiré technique for measuring the geometry of a three-dimensional object is based on the observation of the surface of the object through a plane grating, while a light source projects the shadow of the same grating onto the object. The resulting Moiré is a family of contour lines which measure the distance of the points of the object from the plane of the grating. This method is particularly appealing in a variety of experimental situations, because of its simplicity and the absence of interference with the object under test.

As the Moiré technique provides the geometry of an object, it can also be used to measure the local distortions of the same object under load. The objective of this study is to investigate the feasibility of a Moiré technique for accurate measurements of the distortion of a wind tunnel model under anticipated test conditions in the HIRT facility. The facility and expected test conditions are described in Reference 1. The instrumentation system must provide the capability of measuring local distortions within .05 inches, for a range of deflection on the order of 3" over a 3 foot wing semi-span length. A longitudinal view of the test section is presented in Figure 1. The geometry of the test section is 10 feet wide, 8 feet high and 20 feet long. The test objects are aircraft models mounted on a sector supported sting shown in Figure 1, which allows the experimenter to change the angle of attack during the test. The anticipated overall change of the angle of attack is a total of $15^{\circ}$ . Viewing ports are planned through the tunnel in the inner liner wall as indicated in Figure 1 to provide the instrumentation access. To minimize flow disturbances, the number of the viewing ports and their size must be kept to a minimum. A maximum size of the viewing ports of approximately 6 inches is anticipated. Also, to avoid flow disturbances the grating required by the conventional Moiré technique must be located outside of the test section. These requirements, and in particular the small dimensions of the viewing ports compared to the size of the test model, pose rather severe constraints on the implementation of a Moiré technique and ultimately control the precision of the distortion measurements.

A study of Moiré techniques suitable for this particular application is presented in this report. Section II summarizes the principle of operation of a conventional Moiré approach and the problems arising in its possible use in the HIRT facility. Section III presents a modified version of the Moiré technique which eliminates some of the problems associated with the conventional approach. Section IV discusses a Moiré technique which makes use of a grating applied to the surface of the model and measures the local distortions through a null method. This latter approach offers simplicity of implementation while satisfying the requirement for precision of measurement.

To simplify the study of the various aspects of the Moiré technique, both the recording of the data and the measurement of the distortions are discussed following an optical approach of image analysis. The translation of the optical approach into an automated image measuring, image digitizing and data acquisition system is discussed in Part III of the report.

## 2. CONVENTIONAL MOIRÉ TECHNIQUE

The simplest form of determining the shape of a three-dimensional body by means of a Moiré technique has been discussed in several papers[2,3] and is shown schematically in Figure 2. A plane one-dimensional grating with a uniform spacing $\lambda_x$ between the lines is placed in proximity of the surface S of the body. Assume that a collimated light is used to illuminate the grating and to project the lines of the grating on the surface of the body. A pinhole iris on the focal point of a field lens is used to observe the surface of the body through the same grating.

Represent the grating with a transmittance function

$$T(x) = \frac{1}{2}\left[1 + \cos\frac{2\pi}{\lambda_x}x\right] \tag{I-1}$$

Assume that the grating is placed on the plane x, y and let z(x,y) be the distance of a point of the surface S from the plane of the grating. When the surface of the body is observed through the grating, the observer sees a pattern with an intensity distribution

$$f(x,y) \sim \frac{F}{4}\left\{1+\cos\frac{2\pi}{\lambda_x}x\right\}\left\{1+\cos\frac{2\pi}{\lambda_x}\left[x-(\tan\alpha_1+\tan\alpha_2)z(x,y)\right]\right\} \tag{I-2}$$

where $\alpha_1$ , $\alpha_2$ are the angles of illumination and observation in the plane x,z and F is essentially constant. Equation (I-2) can be written again in the form

$$\begin{aligned} f(x,y) \sim \frac{F}{4}\Bigg\{ & 1+\cos\frac{2\pi}{\lambda_x}x+\cos\frac{2\pi}{\lambda_x}\left[x-(\tan\alpha_1+\tan\alpha_2)z(x,y)\right] \\ & +\frac{1}{2}\cos\frac{2\pi}{\lambda_x}\left[2x-(\tan\alpha_1+\tan\alpha_2)z(x,y)\right] \\ & +\frac{1}{2}\cos\frac{2\pi}{\lambda_x}(\tan\alpha_1+\tan\alpha_2)z(x,y)\Bigg\} \end{aligned} \tag{I-3}$$

Assume now that $z(x,y)$ is a slowly changing function of x and y. In this case the first three cosine terms in Equation (I-3) have a quasi-periodic distribution with a period whose order of magnitude is the spacing $\lambda_x$ of the grating. The argument of the last cosine term, on the contrary, depends only upon $z(x,y)$ and consequently changes slowly with x and y. This last term defines the distribution of the Moiré pattern and the equation of the fringe lines is given by

$$z(x,y) = \frac{n\lambda_x}{\tan \alpha_1 + \tan \alpha_2} \qquad \text{(I-4)}$$

where n is an arbitrary integer. Thus, each fringe line is a contour line of the surface S and the observation of the Moiré pattern provides the geometry of the surface S. Equation (I-4) shows that the smaller the period of the grating, the smaller the depth difference becomes between points of S corresponding to two fringe lines. In a practical situation the elementary formulation of Equation (I-2) has to be improved to account for the finite distance of illumination and observation, the characteristics of the optical systems and the true transmission function of the grating. Several papers have been published on this subject and techniques have been proposed to improve the measurement of the Moiré fringe distribution by eliminating, or filtering out, the presence of unwanted terms in the recorded patterns[4].

In principle the same approach could be used for the instrumentation of the HIRT facility, however, several difficulties would arise in such an approach. These are:

- The grating cannot be located inside the test section in close proximity of the test surface, and only relatively small windows can be built in the wall of the test section for projection of the grating and observation of the test surface. In view of the fact that relatively large angles $\alpha_1$ , $\alpha_2$ are required to obtain a good sensitivity of the measurement, it becomes impossible to observe the test surface through the same grating. Two identical gratings would have to be used at two independent windows (one for projection and one for observation). Such an arrangement would require a highly rigid mechanical system to avoid the effects of distortions and vibrations which could alter the relative position of the two gratings.

- As shown by Equation (I-4) the conventional Moiré technique measures the distance of a point of the test surface from the grating. The objective of the instrumentation for the facility described in Section I is the measurement of the distortion of the model during the test. Thus the distortion of the model would be determined by comparing the Moiré pattern obtained prior to the test. Maximum deflections of the order of one inch are anticipated for the test models while the distance of the model from the gratings would be about four feet or larger. Consequently, the measurement of the distortion would result from a small difference between two large numbers, and an extremely accurate measurement of $z(x,y)$ would be required. A precision better than .05% in the measurement of $z(x,y)$ is required to measure a distortion of the test model within .05 inches.

- In comparing the Moiré patterns obtained prior and during the test a common reference system is required to identify each point of the test model where the distortion has to be computed. The identification of the points of the surface of the test model is not provided by the measuring technique, and reference marks have to be applied to the surface of the model.

- The precision of the Moiré method, for measuring the contour lines of the surface S, is affected by the errors in locating the center lines of the Moiré fringes. Obviously, the broader a Moiré fringe is, the more difficult it becomes to define its boundary and its centerline. This problem is of particular concern, due to the precision which would be required in measuring the test surface distortions from a difference in the location of the fringes in each one of the two Moiré patterns.

- The Moiré pattern described in Equation (I-4) provides only the absolute value of the difference in distance between grating and model at points which belong to consecutive contour lines.

## 3. MODIFIED MOIRÉ TECHNIQUE WITH A PROJECTED GRATING

As pointed out in the previous section, with a conventional Moiré technique, the distortion of the test model is obtained from two independent measurements of the geometry of the model itself prior and during the test. The Moiré technique can be modified to provide directly the measurement of the distortion without the need of an extremely accurate measurement of the geometry of the undistorted model.

In the modified version of the Moiré technique a grating is projected on the surface of the test model. A picture of the projected grating is taken prior to the test and a second picture of the projected grating is taken during the test using the same camera. When the two pictures are superimposed to each other, a Moiré pattern results from the change of the grating projection on the surface of the model during test.

To investigate the basic properties of the modified technique, consider the arrangement of Figure 3. Assume a two-dimensional sinusoidal grating in the plane z = 0 with a transmittance function

$$T(x,y) = \frac{1}{2}\left[\, 1 + \cos\frac{2\pi}{\lambda_x}\cos\frac{2\pi}{\lambda_y}\, y \,\right] \qquad \text{(I-5)}$$

where $\lambda_x$ , $\lambda_y$ are the periods of the grating along the axes x,y respectively. As shown by Figure 3, the principal axes of the grating are parallel to x and y. The undistorted test surface is assumed to be the plane $\zeta' = 0$ of the system of reference $\xi', \eta', \zeta'$.

Assume that the collimated light is used to project the grating in the direction of the axis z on the test surface $\zeta' = 0$. The projection of the grating is seen by an observer located at infinity in the direction of the axis $\zeta$ shown in Figure 3. The axis $\zeta$ is assumed to be in the plane y = 0 at an angle $\Gamma$ with respect to the axis z and the plane of reference $\xi$, $\eta$, $\zeta$ is chosen in such a way that the axis $\eta$ is parallel to y. The plane $\zeta = 0$ is defined as the image plane, and the image of the test surface is given by the projection of the plane $\zeta' = 0$ on the plane $\zeta = 0$.

When the grating is projected on the plane $\zeta' = 0$, the observer sees an image on the plane $\zeta = 0$ whose intensity distribution is given by

$$f_1(\xi,\eta) = \frac{1}{2}\left\{1 + \frac{1}{2}\cos 2\pi\left[\frac{a}{\lambda_x}\xi + \left(\frac{b}{\lambda_x} - \frac{1}{\lambda_y}\right)\eta\right] + \frac{1}{2}\cos 2\pi\left[\frac{a}{\lambda_x}\xi + \left(\frac{b}{\lambda_x} + \frac{1}{\lambda_y}\right)\eta\right]\right\} \tag{I-6}$$

where

$$a = \frac{\cos\theta}{\cos(\theta - \Gamma)} \quad ; \quad b = -\frac{\sin\Gamma\tan\varphi}{\cos(\theta - \Gamma)} \tag{I-7}$$

$\theta$ is the angle of rotation about the axis y which transforms the axis x to an axis x′ parallel to the plane $\zeta' = 0$, as indicated in Figure 3. In Equation (I-7), $\varphi$ is the angle of rotation about the new axis x′, which transforms the system of reference x,y,z into the system of reference $\xi', \eta', \zeta'$ of the undistorted test surface.

The distortion of the test surface considered in this analysis is assumed to be a rotation of the test surface by an angle $\delta$ about an arbitrary axis, parallel to the surface itself. As shown in Figure 3, the distortion is defined as a rotation of the vector $\vec{n}$, perpendicular to the test surface, by an angle $\delta$ in a plane which forms an angle $\alpha$ with the plane $\eta' = 0$.

When the test surface is rotated to its new position, a new image is formed in the image plane $\zeta = 0$. The new image is defined by an intensity distribution $f_2(\xi,\eta)$ which is expressed by an equation similar to (I-6) with an appropriate transformation of the angles $\theta,\varphi$. The superimposition of the two images of the undistorted and distorted test surface has an intensity distribution which is given by

$$f(\xi,\eta)=f_1(\xi,\eta)f_2(\xi,\eta)=\frac{1}{4}\left\{1+\frac{1}{2}\cos\frac{2\pi}{\lambda_x}\frac{\sin\Gamma\cos\alpha\sin\delta}{\Delta(\theta-\Gamma)\cos(\theta-\Gamma)}(\xi-c\eta)+\ldots\right\} \tag{I-8}$$

where

$$c = -\frac{1}{\cos\varphi}\left[\sin\varphi\sin(\theta-\Gamma)+\tan\alpha\cos(\theta-\Gamma)\right] \tag{I-9}$$

and

$$\Delta(\theta-\Gamma) = \sin\delta\left[\cos\alpha\sin(\theta-\Gamma)+\sin\alpha\sin\varphi\cos(\theta-\Gamma)\right] + \cos\delta\cos\varphi\cos(\theta-\Gamma) \tag{I-10}$$

The terms omitted in Equation (I-8) are cosine terms whose periods are of the order of either $\lambda_x$ or $\lambda_y$. If the angle of rotation $\delta$ is sufficiently small, the period of the cosine term on the right hand side of Equation (I-8) is usually much larger than $\lambda_x$. This term represents the Moiré pattern generated by the superimposition of the two images $f_1$ and $f_2$. One observes that the term written in Equation (I-8) is independent of $\lambda_y$ and this is due to the fact that the direction of observation $\zeta$ is perpendicular to the axis y.

The Moiré pattern described in Equation (I-8) is formed by straight lines which are controlled by the equation

$$\xi - c\eta = n\lambda_x\frac{\Delta(\theta-\Gamma)\cos(\theta-\Gamma)}{\sin\Gamma\cos\alpha\sin\delta} \tag{I-11}$$

where n is an arbitrary integer. These lines are parallel to the projection of the axis of rotation of the test surface on the image plane $\zeta = 0$. The Moiré lines are periodically spaced with a period

$$\lambda_f = \lambda_x\frac{\Delta(\theta-\Gamma)\cos(\theta-\Gamma)}{\sin\delta\sin\Gamma\cos\alpha\,(1+c^2)^{1/2}} \tag{I-12}$$

The orientation of the fringe lines in the image plane provides the direction of the axis of rotation of the test surface and the measurement of the spacing $\lambda_f$ between the fringe lines is used in Equation (I-12) to compute the angle of rotation $\delta$ of the test surface. In the particular case of $\delta \ll 1$, the function $\Delta(\theta-\Gamma)$ becomes independent of $\delta$ and Equation (I-12) reduces to

$$\delta \frac{\lambda_f}{\lambda_x} = \frac{\cos \varphi \cos^2 (\theta-\Gamma)}{\sin \Gamma \cos \alpha (1 + c^2)^{\frac{1}{2}}} \qquad \text{(I-13)}$$

The deflection $\epsilon_n$ of an element of the test surface, between two points of the surface which correspond to two consecutive fringe lines, is given by

$$\epsilon_n = \lambda_x \frac{\cos \varphi \cos (\theta-\Gamma)}{\sin \Gamma} \qquad \text{(I-14)}$$

The value of $\epsilon_n / \lambda_x$ is a scale factor which relates the deflection of the element of the test surface to the spacing of the Moiré fringes. This scale factor is a function of all the geometrical parameters which define the orientation of the test surface relative to the direction of illumination and observation. The scale factor has to be measured independently in order to determine the distortion of the test surface from the measurement of the Moiré fringe lines.

Figure 4 shows the value of $\epsilon_n / \lambda_x$ as a function of $\theta/\Gamma$ in the particular case of $\alpha = 0$ and $\varphi \cong 0$. The two curves correspond to two values $\Gamma = 40^\circ$ , $\Gamma = 60^\circ$ of the angle of observation relative to the direction of illumination. Figure 4 shows that an accurate knowledge of the orientation of the undistorted test surface relative to the optical system is required to use the Moiré pattern for a measurement of the test surface distortion. One observes in the same figure that the minimum measurable deflection of the test surface is of the order of the spacing $\lambda_x$ of the grid.

If both source of illumination and point of observation are located at a finite distance from the test surface, a more complicated relationship is found between the fringe lines and the distortion of the test surface. However, the additional

complication does not alter the basic properties of the technique described by Equations (I-8) and (I-12). Thus, the following conclusions are obtained from the analysis presented in this section.

- The Moiré pattern, formed by the two images of undistorted and distorted test surface, provides the direct measurement of the distortion. This is the main advantage of the measuring technique of Figure 3 compared to the conventional Moiré technique described in the previous section. Thus the scheme of Figure 3 is more suitable than the conventional Moiré technique for the particular application investigated in this report.

- The main disadvantage of this technique is that it does not provide a measurement of the geometry of the undistorted test surface. The knowledge of the test surface geometry and its position relative to the optical system are required to determine the local value of the scale factor. Thus an independent measurement of geometry and orientation of the undistorted test surface has to be conducted.

- As it is in the case of the conventional Moiré technique, the measuring arrangement of Figure 3 does not provide the identification of reference points on the test surface and consequently a reference system has to be applied to the surface itself.

- The direct reading of the Moiré fringes in the measuring arrangement of Figure 3 is again affected by the precision by which the center lines of the Moiré fringes can be located in the image plane.

- The reading of the Moiré fringes is affected by an error which derives from the fact that a point of the image plane does not correspond to the same point of the distorted and undistorted test surface. In other words, the beating between the two images of the projected grating does not originate from the displacement of the same point of the test surface.

- The fringe lines provide only the absolute value of the distortion of the test surface between two consecutive fringes. The sign of the distortion has to be determined independently.

## 4. DISTORTION MEASUREMENTS WITH A GRATING APPLIED TO THE TEST SURFACE

### Moiré with the Grating Applied to the Test Surface

The techniques described in the previous sections make use of Moiré patterns generated by the projection of a grating on both distorted and undistorted test surfaces. The main advantage of these techniques is the measurement of the distortion without interference with the experiment and without the need of sensors mounted on the test surface. However, these methods have the disadvantage that they do not provide a reference system of the test surface relative to the Moiré pattern.

A method which eliminates this difficulty and at the same time greatly simplifies the optical system, consists of making the grating an integral part of the test surface. As before, the measurement of the distortion is obtained from the Moiré patterns generated by the superimposition of the pictures of the test surface prior and during the experiment.

The schematic of the measuring arrangement is shown in Figure 5. The plane $z = 0$ is assumed to be the undistorted test surface. A two-dimensional grating is applied to the test surface with the principal axes parallel to x and y respectively. The grating is represented again by an intensity distribution.

$$f(x,y) = \frac{1}{2}\left[1 + \cos\frac{2\pi}{\lambda_x}\, x \cos\frac{2\pi}{\lambda_y}\, y\right] \qquad \text{(I-15)}$$

Assume that the grating is observed at infinity in the direction of the axis $\zeta$. The $\zeta$ axis is oriented at an angle $\Gamma$ with respect to the z axis and the plane $(x, \zeta)$ forms an angle $\Omega$ with respect to the plane $(z,x)$. In the frame of reference $\xi, \eta, \zeta$ of Figure 5 the plane $(\xi, \eta)$ is defined as the image plane and the axes $\xi, \eta$ are assumed to be parallel and perpendicular to the plane $(z, \zeta)$ respectively.

The projection of the grating on the plane $(\xi, \eta)$ has an intensity distribution given by

$$f_1(\xi,\eta) = \frac{1}{2}\left[1 + \cos\frac{2\pi}{\lambda_x}\left(\xi\frac{\cos\Omega}{\cos\Gamma} - \eta\sin\Omega\right)\cos\frac{2\pi}{\lambda_y}\left(\xi\frac{\sin\Omega}{\cos\Gamma} + \eta\cos\Omega\right)\right] \qquad \text{(I-16)}$$

When the test surface is distorted, a new image of the grating is formed in the plane $(\xi,\eta)$ which is represented by an intensity distribution $f_2(\xi,\eta)$ and the Moiré pattern formed by the superimposition of the two images $f_1, f_2$ depends upon the test surface distortion.

As in the previous sections, assume that the distortion of the test surface corresponds to a rotation of the axis z by an angle $\delta$ to the new position $z'$ in the plane which forms an angle $\alpha$ with respect to the plane (z,x), as shown in Figure 6.

To compute the new image of the grating in the plane $(\xi,\eta)$ it is convenient to define the new angles $\Gamma'$, $\Omega'$ which relate the direction of observation $\zeta$ to the distorted surface, as shown in Figure 6. One has

$$\begin{cases} \cos \Gamma' = \cos \Gamma \cos \delta + \cos (\Omega - \alpha) \sin \Gamma \sin \delta \\ \sin \Omega' = \dfrac{\sin (\Omega - \alpha) \sin \Gamma}{\sin \Gamma'} \end{cases} \tag{I-17}$$

and the image of the grating becomes

$$f_2 (\xi,\eta) = \frac{1}{2} \left\{ 1 + \cos \frac{2\pi}{\lambda_x} \left[ a_1 \xi + a_2 \eta \right] \cos \frac{2\pi}{\lambda_y} \left[ a_3 \xi + a_4 \eta \right] \right\} \tag{I-18}$$

where

$$\begin{cases} a_1 = \dfrac{\cos \beta}{\cos \Gamma'} \cos (\Omega' + \alpha) + \sin \beta \sin (\Omega' + \alpha) \\ a_2 = \dfrac{\sin \beta}{\cos \Gamma'} \cos (\Omega' + \alpha) - \cos \beta \sin (\Omega' + \alpha) \\ a_3 = \dfrac{\cos \beta}{\cos \Gamma'} \sin (\Omega' + \alpha) - \sin \beta \cos (\Omega' + \alpha) \\ a_4 = \dfrac{\sin \beta}{\cos \Gamma'} \sin (\Omega' + \alpha) + \cos \beta \cos (\Omega' + \alpha) \end{cases} \tag{I-19}$$

and

$$\sin \beta = \frac{\sin \Omega'}{\sin \Gamma} \sin \delta \tag{I-20}$$

Confine the analysis of the Moiré fringes to the particular case of a one-dimensional grating and small distortions, i.e.,

$$\begin{cases} \lambda_y = \infty \\ \\ \delta << 1 \end{cases} \tag{I-21}$$

In this case, Equations (I-16), (I-18) reduce to

$$\begin{cases} f_1(\xi,\eta) = \frac{1}{2}\left\{1 + \cos\frac{2\pi}{\lambda_x}\left(\xi\frac{\cos\Omega}{\cos\Gamma} - \eta\sin\Omega\right)\right\} \\ \\ f_2(\xi,\eta) = \frac{1}{2}\left\{1 + \cos\frac{2\pi}{\lambda_x}\left[\xi\frac{\cos\Omega}{\cos\Gamma} - \eta\sin\Omega + \delta\left(K_1\xi + K_2\eta\right)\right]\right\} \end{cases} \tag{I-22}$$

where

$$\begin{cases} K_1 = -\cos\left(\Omega - \alpha\right)\cos\Omega\frac{\tan\Gamma}{\cos\Gamma} \\ \\ K_2 = \cos\Omega\tan\Gamma\sin\left(\Omega - \alpha\right) \end{cases} \tag{I-23}$$

Thus, the product of $f_1(\xi,\eta)$ and $f_2(\xi,\eta)$ yields:

$$f_1 f_2 = \frac{1}{4}\left\{1 + \frac{1}{2}\cos\frac{2\pi}{\lambda_x}\delta\left[K_1\xi + K_2\eta\right] + \ldots\right\} \tag{I-24}$$

where the high frequency terms (i.e., the terms whose period is of the order of $\lambda_x$) have been omitted. From Equation (I-24) the fringe lines are straight lines controlled by the equation

$$K_1\xi + K_2\eta = n\frac{\lambda_x}{\delta} \tag{I-25}$$

where n is an arbitrary integer. From Equations (I-23) the distance $\lambda_f$ between fringe lines, i.e., the period of the Moiré pattern, is given by

$$\delta \frac{\lambda_f}{\lambda_x} = \frac{\cos^2 \Gamma}{\cos \Omega \sin \Gamma} \quad \frac{1}{\sqrt{1 - \sin^2 (\Omega - \alpha) \sin^2 \Gamma}} \qquad \text{(I-26)}$$

The axis of rotation of the test surface is the straight line

$$x + y \tan \alpha = 0 \qquad \text{(I-27)}$$

in the plane (x,y). The projection of the axis of rotation Equation (I-27) in the image plane is given by the equation

$$\frac{\cos (\Omega - \alpha)}{\cos \Gamma} \xi - \sin (\Omega - \alpha) \eta = 0 \qquad \text{(I-28)}$$

Thus, by virtue of Equation (I-23), (I-25), the fringe lines are parallel to the image of the axis of rotation, and their spacing provides the value of the angle of rotation.

As noted earlier, using a technique based on the projection of the grating on the test surface, the Moiré is independent of a rotation of the test surface about an axis perpendicular to the surface itself. A different situation is encountered when the grating is an integral part of the surface. Assume in Figure 6 that the test surface rotates by an angle $\theta$ about the axis z. The projection of the rotated one-dimensional grating in the image plane $(\xi,\eta)$ has an intensity distribution given by

$$f_{2\theta}(\xi,\eta) = \frac{1}{2} \left\{1 + \cos \frac{2\pi}{\lambda_x} \left[\xi \frac{\cos (\Omega - \theta)}{\cos \Gamma} - \eta \sin (\Omega - \theta) \right]\right\} \qquad \text{(I-29)}$$

The superimposition of the two images is given by the product of Equation (I-29) and the first equation of system (I-22) . For small values of $\theta$ ($\theta \ll 1$) it yields

$$f_1 f_{2\theta} = \frac{1}{4} \left\{1 + \frac{1}{2} \cos \frac{2\pi}{\lambda_x} \theta \left[\xi \frac{\sin \Omega}{\cos \Gamma} + \eta \cos \Omega \right] + \ldots\right\} \qquad \text{(I-30)}$$

The terms omitted in Equation (I-30) have a period of the order of $\lambda_x$. In Equation (I-30) one observes that the fringe lines are given by the equation

$$\xi \frac{\sin \Omega}{\cos \Gamma} + \eta \cos \Omega = n \frac{\lambda_x}{\theta} \tag{I-31}$$

where again n is an arbitrary integer. Equation (I-31) shows that in the particular case of $\Gamma = 0$ (observation perpendicular to the test surface) the fringe lines in the image plane are perpendicular to the images of the images of the lines of the grating. The period of the Moiré pattern is given by

$$\theta \frac{\lambda_f}{\lambda_x} = \frac{\cos \Gamma}{\sqrt{1 - \sin^2 \Gamma \cos^2 \Omega}} \tag{I-32}$$

Thus an advantage is gained in that the physical application of the grating can be used to measure the distortion of the test surface as well as a rotation of the surface in its own plane.

The preceding analysis assumes that the image plane is located at infinity in the direction of the axis $\zeta$. As a consequence the Moiré pattern is insensitive to a translation of the test surface in any direction.

In practice, a camera would be used to record the image of the test surface and the Moiré pattern would depend upon the distance between camera and test surface and the characteristics of the optics of the camera as well. Assume the simple case schematically presented in Figure 7. $S_1$ is the undistorted test surface, and $S_i$ is the image plane. $\zeta$ is the axis of the optical system and 0 is the position of the iris diaphragm of the camera. A one-dimensional grating is applied to $S_1$ in a narrow strip along the axis x. The origins of both axes x, $\xi$ in Figure 7 are taken at the intersection of the optical axis with $S_1$ and $S_i$ respectively. In the plane of Figure 7 the $\xi$ coordinate of the image point $P_i$ is related to the x-coordinate of the object point P by the equation

$$\xi = - \zeta_1 \cos \Gamma \frac{x}{\zeta_2 + x \sin \Gamma} \tag{I-33}$$

and the image along the axis $\xi$ of the grating has a nonuniform spacing $\lambda_\xi$ between the lines, which is given by

$$\lambda_{\xi 1} = \lambda_x \frac{\zeta_1 \zeta_2 \cos \Gamma}{\left[\zeta_2 + x \sin \Gamma\right]\left[\zeta_2 + (x + \lambda_x) \sin \Gamma\right]} \tag{I-34}$$

where in a practical situation

$$\lambda_x << \zeta_2 \tag{I-35}$$

By virtue of Equations (I-33) and (I-35), Equation (I-34) can be written in terms of the $\xi$ coordinate of the image plane

$$\lambda_{\xi 1} = \lambda_x \frac{(\zeta_1 \cos \Gamma + \xi \sin \Gamma)^2}{\zeta_1 \zeta_2 \cos \Gamma} \tag{I-36}$$

Assume now that the test surface is rotated by an angle $\delta$ about the axis y and is translated along the axis $\zeta$ by $\epsilon$ as shown in Figure 7. Both $\delta$ and $\epsilon$ are assumed to be small. The spacing along the axis $\xi$ between the lines of the image grating becomes

$$\lambda_{\xi 2} \sim \lambda_{\xi 1} \left[1 - \frac{\epsilon}{\zeta_2} + \frac{\delta}{\cos \Gamma}\left(\sin \Gamma + \frac{2x}{\zeta_2}\right)\right] \tag{I-37}$$

Thus the fringes of the Moiré pattern formed by the superimposition of the images of the test surface have a spacing $\lambda_f$

$$\frac{\lambda_f}{\lambda_x} \sim \frac{\zeta_1 \zeta_2^2 \cos^2 \Gamma}{(\zeta_2 + x \sin \Gamma)^2} \frac{1}{\epsilon \cos \Gamma - \delta (\zeta_2 \sin \Gamma + 2x)} \tag{I-38}$$

One observes that the spacing of the Moiré fringes is not uniform and $\lambda_f$ decreases as the distance of the object point from the image plane increases. The Moiré pattern is now dependent upon a rotation as well as a translation of the test surface. This property can now be used to analyze the data as described in the following section.

Null Method Based on the Moiré Technique

Equations (I-26) and (I-28) provide the measurement of the angular distortion of the test surface, based on the direct reading of both orientation and spacing of the Moiré pattern. Equation (I-28) gives the value of $\alpha$ and Equation (I-26) provides the average value of $\delta$ between two fringes of the Moiré pattern. The sensitivity of the measurement is determined primarily by the period $\lambda_x$ of the grating and the accuracy depends upon the knowledge of the geometrical parameters $\Gamma$, $\Omega$.

Both sensitivity and accuracy of the measurements can be increased by using the Moiré pattern as a null method. A simple analysis of the null method can be performed assuming a one-dimensional case where $\Omega = 0$ and the axis of rotation of the test surface coincides with the y-axis of Figure 5 ($\alpha = 0$). Assume a one-dimensional grating ($\lambda_y = \infty$), and let $I_1$ be the image of the grating prior to the distortion of the test surface. The image of the grating after the distortion of the test surface is denoted by $I_2$. The intensity distributions of $I_1$ and $I_2$ are given by Equations (I-22) with $\Omega = \alpha = 0$.

Assume that $I_1$ is projected on an observation plane, as shown in Figure 8, at an angle $\Gamma_1$ close to the original angle $\Gamma$ of observation of the test surface. The projection of $I_1$ on the observation plane has an intensity distribution

$$\bar{f}_1 = \frac{1}{2}\left[1 + \cos \frac{2\pi}{\lambda_x} \bar{x} \frac{\cos \Gamma_1}{\cos \Gamma}\right] \qquad \text{(I-39)}$$

where $\bar{x}$ is the coordinate in the observation plane as shown in Figure 8. Assume now that the image $I_2$ of the distorted test surface is projected on the observation plane at an angle

$$\Gamma_2 = \Gamma_1 - \bar{\delta} \qquad \text{(I-40)}$$

The intensity distribution of the projection of $I_2$ on the observation plane is

$$\bar{f}_2 = \frac{1}{2}\left[1 + \cos \frac{2\pi}{\lambda_x} \bar{x} \frac{\cos (\Gamma_1 - \bar{\delta})}{\cos (\Gamma - \delta)}\right] \qquad \text{(I-41)}$$

With the assumption of small values of both $\delta$ and $\bar{\delta}$ the superimposition of $f_1$, $f_2$ yields

$$\bar{f}_1\bar{f}_2 = \frac{1}{4}\left[1 + \frac{1}{2}\cos\frac{2\pi}{\lambda_x}\bar{x}\,\frac{\cos\Gamma_1}{\cos\Gamma}\,(\bar{\delta}\tan\Gamma_1 - \delta\tan\Gamma) + \ldots\right] \tag{I-42}$$

where the terms with period of the order of $\lambda_x$ have been omitted. Thus a Moiré pattern is formed in the observation plane and the spacing between the fringe lines approaches infinity when

$$\bar{\delta} = \delta\tan\Gamma\cot\Gamma_1 \tag{I-43}$$

Equation (I-43) provides the principle of the null method in the measurement of the deflection angle $\delta$. If the value of $\Gamma$ is known and $\Gamma_1 = \Gamma$ the value of $\bar{\delta}$ is precisely the deflection angle $\delta$ since the projections $I_1$ and $I_2$ reconstruct the original grating on the test surface. In the measuring scheme of Figure 8 the fringe lines get closer to each other as $\delta$ deviates more and more from $\bar{\delta}$ and they get farther apart as $\bar{\delta}$ approaches $\delta$. The accuracy of the measurement depends upon the accuracy by which $\Gamma$ is known. Assume that $\Gamma_1$ differs from $\Gamma$ by a small angle $\psi$

$$\Gamma_1 = \Gamma + \psi \quad (|\psi| \ll 1) \tag{I-44}$$

The error $\bar{\delta} - \delta$ of the measurement is given by

$$\frac{\bar{\delta} - \delta}{\delta} = -\frac{2\psi}{\sin 2\Gamma} \tag{I-45}$$

The result shows that $\Gamma = 45^\circ$ is the the optimum angle of observation which provides the maximum accuracy. At $\Gamma = 45^\circ$ an error of 1% in the estimate of $\Gamma$ results in an accuracy better than 2% in the measurement of the deflection angle $\delta$.

In an actual test condition the distortion of the test surface generates a change of the local radius of curvature. As a consequence, when the images $I_1$, $I_2$ are projected on the observation plane, the Moiré pattern cannot be cancelled completely in the entire plane. Assume the case of Figure 9 where the distortion of the test surface transforms the plane $S_1$ into the curved surface $S_2$. A point $P_1$ of the undistorted surface $S_1$ moves to the new position $P_2$ in the distorted surface $S_2$. To measure the angle $\delta$ between $S_1$ and the tangent to $S_2$ at $P_2$, the two images $I_1$, $I_2$ have to be properly positioned in the scheme of Figure 8 in such a way as to bring into

coincidence on the observation plane the projections of the two images of $P_1$ and $P_2$. It is important to observe that each point of the test surface is readily identified in this measuring technique because its position is provided by any particular line of the grating applied to the surface.

Once the projections of the two images of $P_1$ and $P_2$ are brought into coincidence on the observation plane, the axis of projection $I_2$ is rotated as in Figure 8. Again the fringe lines get farther apart from each other as $\bar{\delta}$ approaches the value of $\delta$. However, the condition $\bar{\delta} = \delta$ is obtained when the spacing between fringes attains a maximum value given by

$$\lambda_{fm} \cong \sqrt{\frac{2\lambda_x r}{\tan \Gamma}} \qquad \text{(I-46)}$$

where r is the radius of curvature of the distorted test surface at $P_2$. Assume a typical situation where $\Gamma = 45°$, $\lambda_x = .03$ inches and a value of r corresponding to a deflection of the order of 1 inch over a length of the test surface of 3 feet. One has $r \cong 650$ inches and Equation (I-46) gives a value of $\lambda_{fm}$ of ~6 inches, which is very large compared to $\lambda_x$ ($\lambda_{fm}/\lambda_x \sim 200$). Thus the change of the radius of curvature induced by a typical distortion of the test surface, does not affect in any appreciable way the sensitivity of the null method.

So far the null method has been discussed with the image plane located at infinity. Assume again that $I_1$, $I_2$ are the two images of the grating applied to the test surface. The basic scheme of Figure 8 is used to project both images on a common observation plane. In the projection of the image $I_1$ of the undistorted surface, the optical axis of the projection system is oriented at the angle $\Gamma_1 = \Gamma$ with respect to the normal to the observation plane, and a distance $\zeta_2$ is maintained between the iris diaphram and the interception of the optical axis with the observation plane. Thus the projection of $I_1$ regenerates the original grating with a period $\lambda_x$.

Assume now that the image $I_2$ of the distorted surface is projected on the observation plane using an identical projection system and let $\Gamma_2$ , $\bar{\zeta}_2$ be the angle of projection and the distance

of the iris diaphram from the interception of the new optical axis with the observation plane. One can write

$$\Gamma_2 = \Gamma - \bar{\delta} \ , \ \bar{\zeta}_2 = \zeta_2 + \bar{\epsilon} \tag{I-47}$$

where both quantities $\bar{\delta}$ , $\bar{\epsilon}$ are assumed to be small compared to $\Gamma$ and $\zeta_2$ respectively. The projection of $I_2$ on the observation plane generates a grating with a non-uniform spacing $\bar{\lambda}_x$ between lines

$$\bar{\lambda}_x = \lambda \left[ 1 + \frac{1}{\zeta_2} (\bar{\epsilon} - \epsilon) + (\bar{\delta} - \delta) \left( \tan \Gamma - 2 \frac{\zeta_1 \sin \Gamma - \xi \cos \Gamma}{\zeta_1 \cos \Gamma + \xi \sin \Gamma} \right) \right] \tag{I-48}$$

where the coordinate $\bar{x}$ in the observation plane is related to the coordinate $\xi$ in the plane of image $I_2$ by the equation

$$\bar{x} = - \xi \frac{\zeta_2}{\zeta_1 \cos \Gamma + \xi \sin \Gamma} \tag{I-49}$$

When both images $I_1$, $I_2$ are simultaneously projected on the observation plane, the spacing of the Moire fringes is

$$\frac{\bar{\lambda}_f}{\lambda} = \frac{1}{\frac{1}{\zeta_2} (\bar{\epsilon} - \epsilon) + (\bar{\delta} - \delta) \left( \tan \Gamma - 2 \frac{\zeta_1 \sin \Gamma - \xi \cos \Gamma}{\zeta_1 \cos \Gamma + \xi \sin \Gamma} \right)} \tag{I-50}$$

As the angle $\bar{\delta}$ approaches $\delta$ the Moiré pattern becomes uniform with a spacing between fringes

$$\left( \frac{\bar{\lambda}_f}{\lambda} \right)_{\bar{\delta} = \delta} = \frac{\zeta_2}{\bar{\epsilon} - \epsilon} \tag{I-51}$$

Finally when the distance $\bar{\zeta}_2$ approaches the original value $\zeta_2 + \epsilon$ the fringe lines get farther apart from each other. Thus, when the Moiré pattern is cancelled in the observation plane, the two correction parameters $\bar{\delta}$ , $\bar{\epsilon}$ provide the values of both rotation and displacement of the test surface.

Measurement of Geometry and Position of the Test Surface

Both the Moiré pattern analyzed in Section 4 and the null method of Section 4 as well, require the knowledge of the geometry of the test surface and its position relative to the observer in order to provide the measurement of the distortion.

The same grating applied to the test model can be used to acquire this information. In principle, since the period $\lambda_x$ of the grating is a known quantity, by observing the test model from a single point at a finite distance, both geometry and position of the test surface can be measured. Such a procedure would require an extremely accurate measurement in the image plane of $\lambda_\xi$ and the rate of change of $\lambda_\xi$ . A better approach is a stereoscopic technique with a second camera which records an additional image of the test surface from a widely different angle of observation as shown in the scheme of Figure 10. Let $I_1$ and $I_1'$ be the images obtained with the primary camera C and the auxiliary camera C' respectively, and assume that $I_1$, $I_1'$ are projected on a common observation plane at the same angle $\varphi$ of Figure 10, and from the same relative position S of the two cameras C, C'. For simplicity assume the two-dimensional case shown in Figure 11 where $S_a$ represents the observation plane and the dotted line $\bar{S}$ represents the position that the projection plane should have in order to coincide with an element of the test surface S, about a point P.

It is apparent that a Moiré pattern is formed in the plane $S_a$ by the superimposition of the projected $I_1$ and $I_2'$ . In Figure 11, $P_a$ , $P'_a$ represent the projections on $S_a$ of the two images of the same point P of the test surface. A point P of the test surface is automatically identified with the grating applied to the surface, and the position of P is given by the number of the line of the grating passing through P. With a translation of the projection surface $S_a$ to the new position $S_b$, the two points $P_a$, $P_a'$ are brought into coincidence and consequently $P_a$, $P_a'$ coincide with the point P of $\bar{S}$. Still a Moire pattern is observed on $S_b$ , because the projections of $S_b$ of the two images of the original grating have different spacings $\lambda_a$ , $\lambda_a'$ as shown in Figure 10 and the spacing $\lambda_{fb}$ of the Moire fringe on $S_b$ at P is

$$\frac{1}{\lambda_{fb}} = \frac{1}{\lambda_b} - \frac{1}{\lambda_b'} \qquad \text{(I-52)}$$

As the surface $S_b$ is rotated about P, $\lambda_{fb}$ decreases or increases depending upon whether the angle $\delta_b$ increases or decreases respectively, and the maximum value of $\lambda_{fb}$ is found when $S_b$ coincides with $\bar{S}$. As a consequence the null method applied to the Moiré pattern can be used at each point of the test surface $S_1$ to determine its geometry and its position relative to camera C.

Implementation of the Measuring Technique

The measuring technique based on the use of a grating applied to the test surface is schematically illustrated in Figure 12. Prior to the test both cameras C and C' are used to obtain the images $I_1$ and $I_1'$ of the undistorted test surface. The Moiré resulting from the superimposition of $I_1$ and $I_1'$ projected on a common observation plane is analyzed to provide the geometrical parameters of the undistorted test surface. During the test a picture $I_2$ of the distorted test surface is obtained with camera C. The Moiré resulting from the superimposition of $I_1$ and $I_2$ projected on the observation plane measures the distortion of the test surface. The Moiré is analyzed with the input provided by the measurement of the geometrical parameters of the undistorted surface. The null method described in Section 4 is used in the analysis of the Moiré to accurately measure the local distortion.

From the analysis presented in this section, the following conclusions are obtained:

- The null method, applied to the Moire pattern formed by the projection of the two images, $I_1$ , $I_2$ of the undistorted and distorted test surface, provides the direct measurement of the distortion.

- The null method is not affected by the errors of the measurement of the spacing between fringes. This is an important advantage of the null method compared to the conventional Moiré technique. Furthermore, the null method eliminates the error introduced in the modified Moiré technique of Section 3 which does not compensate for the displacement of the test surface. Consequently, a higher precision is achieved with the null method compared to the techniques based on a direct reading of Moiré patterns.

- The use of a grating as an integral part of the test surface provides an automatic identification of reference points on the test surface and makes it possible to properly align the independent images for the distortion measurement.

- As in the modified Moiré technique, the null method requires an independent measurement of the geometry of the test surface and its position relative to the optical system. However, the grating applied to the surface can be used to obtain this information and the measurement of the pertinent geometrical parameters can be performed with the aid of an additional camera. Again, a null method applied to the Moiré pattern, as described in the previous section, can be used to achieve the maximum precision in the measurement of position and orientation of each element of the test surface.

- Magnitude and size of $\epsilon$ , $\delta$ are measured with Equation (I-50) when the Moiré pattern is cancelled. Consequently, the distortion of the test surface is uniquely defined in the null method technique.

## Experimental Study of the Moiré Pattern

To perform an experimental study of the Moiré patterns generated with a grating applied to the test surface a fixture was built to support a test surface of dimensions similar to those of the anticipated test models of the HIRT facility. The support of the test surface was designed to vary the orientation and position of the test surface and to apply known distortions to prescribed sections of the surface itself. A picture of the fixture is presented in Figure 13 which shows the rotating platform with the support of the test surface. The test surface itself is a $^3/_{32}$ inches thick aluminum rectangular sheet 10 x 36 inches. A set of six screws attached to the support are used to control the distortion of the surface. Also shown in Figure 13 is the camera and its support used to change the angle of observation of the test surface. A Graflex camera equipped with a 1:4.5, f = 135 mm lens is used to photograph the test surface. In the arrangement of Figure 13 the distance of the image plane from the interception of the optical axis with the plane of the test surface can be adjusted to a maximum of approximately 4 feet. Thus the arrangement of Figure 13 makes use of test surface dimensions and camera to model distances close to the measuring arrangement for the anticipated facility.

For convenience Polaroid film, Type 57, in the 4 x 5 format was used in these measurements. Although higher resolution films are available this film proved to be adequate to illustrate the basic characteristics of the Moire and to confirm the measured data with the theoretical results.

Based on the considerations presented in Section 4.1, a one-dimensional grating with a period $\lambda_x$ = .037 inches was selected to be applied to the test surface. The grating is formed with black lines on white background with a one-to-one ratio of line width and spacing. Strips of the grating are applied to the test surface as shown in Figure 14. To simulate the superimposition of the two images of the grating, according to the measuring arrangement of Figure 5, a double exposure of the same photographic plate is used to record the images of the test surface in the undistorted and distorted condition. A typical result is shown in Figure 15, obtained with the optical axis of the camera at approximately 45° with respect to the normal to the undistorted surface. The distortion of the test surface corresponding to Figure 15 is a rotation of the element of surface covered by the first strip of grating about an axis parallel to the narrow side of the test surface. In the frame of reference defined in Figure 7 the element of surface rotates by an angle $\delta$ = .04 radians about an axis located at x = - 10.33". The total deflection over the length of the first strip of grating is about .24 inches. In Figure 15 the misalignment of the two pictures due to the distortion of the test surface can be observed, and ten fringe lines are found in the overlapping portions of the first strip of grating. The measured center to center distance $\lambda_f$ between the fringe lines of Figure 15 is plotted as points in Figure 16 vs the distance $x_o$ - x from the free end of the test surface. The Moiré of Figure 15 corresponds to the combined effect of rotation and translation. The solid line of Figure 16 presents the theoretical values of $\lambda_f$ obtained from Equation (I-38) for the corresponding values of $\delta$ and $\epsilon$. One observes that experimental and calculated values are within 10% or each other. The deflection of the test surface between two points corresponding to two consecutive fringe lines is about .027 inches. Thus the arrangement of Figure 13 and the selection of this particular grating allow the measurement of distortion values to .025 inches.

Figures 17, 18 show the Moiré patterns obtained with three .75 inches wide strips of the same grating. Figure 17 corresponds to a rotation about an axis parallel to the narrow side of the test surface. Thus the fringe lines are perpendicular to the strips of grating. Figure 18 corresponds to a twist of the test surface where the main axis of the surface itself does not move in the distorted condition. One observes in Figure 18 the Moiré patterns in the upper and lower gratings induced by the twist of the test surface. One fringe, essentially parallel to the main axis of the test surface is generated in the middle strip.

Finally, Figures 19a, 19b, illustrate a simulation of the partial cancellation of the Moiré pattern in the null method for measurements of both rotation and translation of the test surface. Figure 19a is a double exposure of the distorted and undistorted test surface. The distortion at the position of the gratings corresponds to a rotation by anangle of approximately .04 rad about an axis parallel to the narrow side of the test surface and a translation of approximately .25 inches along the optical axis of the camera. Figure 19b shows the image of the undistorted surface with the camera in its original position, superimposed to the image of the distorted surface with the camera axis rotated by .04 rad and displaced by .20 inches. No compensation has been introduced for translation in the plane of the test surface. The double exposure of the middle grating in Figure 19a shows ten Moiré fringes, which, in the partial compensation of Figure 19b reduce to 4. In Figure 19b one can observe the strong misalignment of the brackets holding the test surface, which is induced by the cancellation of the Moiré pattern at the position of the gratings. It is also worthwhile pointing out that the spacing between fringes is Figure 19b has become almost uniform, which is consistent with the fact that an almost total correction of the angular distortion has been achieved in the partial cancellation of the Moiré pattern. These measurements show the feasibility of the measuring technique based on the application of the grating to the test surface, and the precision which can be achieved. In particular, the measurements illustrate the logic to be followed in generating a data reduction procedure based on the null method. Another key feature illustrated by the measurements is the simplicity of the implementation of the technique.

# PART II

## INSTRUMENTATION AND MEASURING PROCEDURE

### 1. INTRODUCTION

The comparative study of the techniques presented in Part I indicates that the method of applying the grating directly to the surface of the test model is the best approach to the use of a Moiré technique in the instrumentation of the test section of the HIRT facility. The same grating is used for the measurement of the geometry of the test model as well as its distortion during the test. As shown both in the theoretical discussion and the measurements described in Part I, distortions well within the desired value of .05 inches can be accurately measured. The discussion presented in Part I is based on a manual approach where the observer makes use of an optical system both to record the image of the grating and to analyze the image and determine the local distortions of the test model.

The anticipated running time of the HIRT facility is 2.5 seconds during which the local distortions of the test models have to be measured as the angle of attack is changed either continuously or in steps. As a consequence an automated data recording, data analysis and computer system is required. This part of the report shows how the measuring approach analyzed in Section 4 of Part I can be easily translated into an automated instrumentation system.

## 2. DATA RECORDING SYSTEM

Figure 12 illustrates the schematic of the recording cameras and the approach recommended for the measurement of the test model distortions and the measurement of the test model geometry and orientation as well. Camera C provides the two images $I_1, I_2$ in the undistorted and distorted condition, respectively, for the distortion measurements. Camera C′ provides the additional image $I_1'$ of the undistorted model for the geometry and orientation measurements.

The measuring technique requires a grating built into the surface of the model. A .037 inches period should be used to allow measurements of distortions within the specified value of .050 inches. The grating should have approximately a one-to-one ratio of line width and spacing, and it could be applied in strips aligned with the points of the model where the measurements are planned as indicated in the scheme of Figure 20.

On the basis of the specified requirments and as a result of a survey of available equipment it is recommended that the two cameras:

- be motion picture cameras utilizing 35 mm film
- have a maximum speed in the range of 200 frames per second
- be pin registered for maximum resolution of the image and accuracy in subsequent measurements
- have provision for recording test data, like time base and test indentification inputs

Cameras satisfying these requirements are commercially available with film capacity up to 1000 ft. in magazine. The 35 mm format is consistent with the required resolution. A 70 mm film size was considered but found impractical because it would require a specially designed camera system. An f1:2.0 lens for these cameras, capable of resolving the .037 grating built into the surface of the model, is available on an off-the-shelf basis.

Available cameras have provision for the above mentioned inclusion of test data on the images of the gratings. Several variations are possible in the data recording systems where the information can be placed on the film in the form of either coded readout or binary coded decimal readout. The selection of the best system would have to be made during the actual design phase of the instrumentation.

New films are constantly being introduced by manufacturers while others are being dropped. The two best currently available films, which fit the resolution requirements have the following characteristics:

| TYPE* | ASA | DEVELOPMENT |
|---|---|---|
| #2491 | 64 | Negative - #D19 at 95°F, 2 minutes |
| #2496 | 125 | Negative - #D19 at 95°F, 1 minute |

"On site" processing of the film should be considered for faster results and better control of the processing techniques.

The mounting of the cameras does not appear to present any special problem. A simple, but sturdy, frame could be used to hold both cameras. Two openings, approximately 6 inches in diameter would be required in the inner wall of the test section for observation of the grating, and provisions for appropriate openings should be made in the outer wall of the facility to permit access to the camera system.

Finally, consideration must be given to the lighting of the test model, as required by the recording cameras. Strobe lighting, as against tungsten, is recommended to provide a maximum resolution of the grating patterns. Typical commercially available stroboscopic light sources have the following characteristics:

0 to 1,000 flashes per second

1.25 to 7.0 μsec flash duration

3,000,000 beam candle output maximum

It is possible to use the arrangement shown in Figure 21 to minimize the number of ports in the inner wall of the facility. In this arrangement a beam splitter would be used to allow both the light source and the camera to use the same optical axis.

* Eastman Kodak Co., Rochester, N.Y.

## 3. IMAGE DIGITIZING SYSTEM

In order to obtain the surface deflection it is necessary to convert the image of the grating as recorded on film to a digital form suitable for input to a data reduction software package. In particular the period of the image grating must be read from the film. A typical programmable film scanning system for accomplishing this is outlined in Figure 22. The scanner reads the photograph converting it to an analog form and displays it on a screen. An analog-to-digital converter then obtains the grating period and stores it on magnetic tape, which can be input to the data reduction software. A programmable controller is used to interact with the scanner for selectable point scanning, image rotational orientation and possible interaction with the data analyzing software.

If the test surface grating lines are about .020" thick and 35 mm film is used the grating lines on the film will have a thickness of about .001". Programmable film scanners are available commercially which have a resolution down to .0005 inches and are capable of distinguishing up to 64 levels of grey. These units typically consist of a light source, optical assembly, automatic roll-film transport, photomultiplier electronics, image display, analog-to-digital converter and the programmable controller. The controller can be operated either manually or by a program, with input or program modes operator applied through a teletype. Most scanner manufacturers also have 9 and 7 track magnetic tape units available which are compatible with their image digitizers.

Therefore, it is obvious that state-of-the-art equipment is available which can automatically

1) select a particular portion of the film frame for scanning
2) rotationally orient the frame to a predetermined reference and record the angle of rotation
3) digitize the image grating period
4) display the image on a screen
5) store the angle of rotation and grating period on magnetic tape for software reduction

## 4. DATA REDUCTION SOFTWARE

The digital data produced by the image analyzing equipment must be properly processed to obtain the rotational distortion ($\delta$) and translational motion of the test surface ($\epsilon$). Figure 23 presents a representative flow diagram of an appropriate software package.

The test surface grid period ($\lambda$) and the camera focal length ($\zeta_1$) are known constants of the instrument system. Initial values of rotational distortion ($\bar{\delta}_o$) and translation ($\bar{\epsilon}_o$) must be chosen along with the value of the coordinate on the image plane at which the optical axis intersects the image plane ($\xi_o$ normally = 0). The choice of step sizes in $\bar{\delta}$, $\bar{\epsilon}$ $\xi_o$ is also required.

The orientation of the undistorted test surface defined by the angle between the optical axis and the test surface ($\Gamma$) and the distance between the optical center and the surface measured along the optical axis ($\zeta_2$), is obtained from the analysis of photographs from both camera C and C′ in the undistorted condition. The image analyzing system provides the grid period of the distorted image (picture) plane ($\lambda_\xi$) and the angle of rotation in the plane of the image ($\theta$) necessary to align the undistorted and distorted images of the grid.

Having chosen values of $\bar{\delta}$ and $\bar{\epsilon}$ , the arbitrary orientation of the distorted surface is given by

$$\Gamma_2 = \Gamma - \bar{\delta}$$

$$\bar{\zeta}_2 = \zeta_2 + \bar{\epsilon} \qquad \text{(II-1)}$$

Then the period of the observed grid on the distorted test surface can be computed at $\xi_o$

$$\bar{\lambda}_x(\xi) = \lambda_\xi \frac{\zeta_1 \bar{\zeta}_2 \cos \Gamma_2}{(\zeta_1 \cos \Gamma_2 + \epsilon \sin \Gamma_2)^a} \qquad \text{(II-2)}$$

The Moiré fringe spacing is easily computed from

$$\bar{\lambda}_f(\xi) = \frac{1}{\left(\frac{1}{\bar{\lambda}_x} - \frac{1}{\lambda}\right)} \qquad \text{(II-3)}$$

Similarly $\bar{\lambda}_f$ can be computed at $\xi = \xi_o + \Delta\xi$ .

The elimination of $\Gamma$ and $\bar{\zeta}_2$ from Equation (II-3) allows it to be rewritten in the form

$$\bar{\lambda}_f = \frac{\lambda}{\frac{1}{\zeta_2}(\bar{\epsilon} - \epsilon) + (\bar{\delta} - \delta)\left(\tan\Gamma - 2\,\frac{\zeta_1 \sin\Gamma - \xi\cos\Gamma}{\zeta_1\cos\Gamma + \xi\sin\Gamma}\right)} \qquad \text{(II-4)}$$

It is evident that if $\bar{\delta} = \delta$ , $\bar{\lambda}_f$ will be independent of $\xi$. Therefore, the differences between $\bar{\lambda}_f$ , computed from Equation (II-3) at $\xi_o$ and $\xi_o + \Delta\xi$ , as well as at $\xi_o + \Delta\xi$ and $\xi_o - \Delta\xi$ are required to be less than a small number $(\alpha_1)$. If they are not, $\bar{\delta}$ is incremented in the proper direction until $\bar{\lambda}_f$ at $\xi_o$ , $\xi_o + \Delta\xi$ and $\xi_o - \Delta\xi$ is constant to desired accuracy. The final value of $\bar{\delta}$ can then be considered to be the surface deflection $\delta$. In the special case where $\bar{\lambda}_f(\xi_o) = \bar{\lambda}_f(\xi_o + \Delta\xi)$ but $\bar{\lambda}_f(\xi_o + \Delta\xi) \neq \bar{\lambda}_f(\xi_o - \Delta\xi)$, the value of $\Delta\xi$ is halved and the process repeated.

With $\bar{\delta} = \delta$, the remaining term in Equation (II-4) shows that $\bar{\lambda}_f$ becomes infinite when $\bar{\epsilon} = \epsilon$ , i.e., the fringe lines disappear (are nulled) when the proper deflection is obtained. Therefore, $1/\bar{\lambda}_f$ is required to be less than a small number $(\alpha_2)$. If it is not, $\bar{\epsilon}$ is incremented in the proper direction. Once the condition is satisfied $\bar{\epsilon}$ is considered equal to the surface translation $\epsilon$ and the results are output.

In the preceding sections, the data recording and reduction system associated with the recommended model deformation measurement technique has been delineated. The recommended system allows deformation data reduction compatible with the anticipated, one hour duty cycle, of the HIRT facility.

# PART III

# RESULTS AND RECOMMENDATIONS

## 1. INTRODUCTION

This part summarizes the overall results of this program and presents recommendations for the HIRT facility model deformation measuring system.

## 2. RESULTS OF THE STUDY

### Conventional Moiré Technique

The use of a conventional Moiré technique based on a single grating is precluded by the configuration and dimensions of the anticipated test arrangement and by the permissible size of the viewing ports in the wall of the test section.

### Modified Moiré Technique With Two Gratings

A conventional Moiré technique could be used with two independent gratings located outside of the test section; one for projection and the second for observation. The distortion of the test model would be obtained by comparing the Moiré patterns obtained in both undistorted and distorted conditions.

- The technique requires an extremely accurate measurement of the contour lines in both Moiré patterns.
- The resolution in determining the center lines of the Moiré fringes is poor.
- The Moiré contour lines provide only the absolute values of the difference in distance between model surface and grating.
- No identification of the points of the test model surface is provided by the technique.
- The measurement is affected by a relative motion of the two gratings one with respect to each other.
- The technique cannot measure a rotation in the plane of the test surface.

In conclusion, this technique does not appear to be suitable for the anticipated instrumentation.

Modified Moiré technique with One Grating

A modified Moiré could be used to obtain a direct measurement of the distortion of the test model. The image of a grating is projected on the surface of the model and two pictures are taken of the projected grating in both undistorted and distorted conditions. The Moiré resulting from the superimposition of the two pictures would provide the measurement of the local distortion. The following conclusions are reached:

- The technique requires an independent accurate measurement of the geometry and position of the test model in its undistorted condition.
- The technique is affected by a poor resolution in the determination of the center lines of the Moiré fringes.
- The technique provides only the magnitude, but not the sign of the local distortion of the model.
- The technique is affected by the lack of common reference points in the two images.
- The technique cannot measure a rotation in the plane of the test surface.

In conclusion, the technique does not appear to be adequate, in spite of its advantage of providing a direct measurement of the distortion.

Moiré Technique With a Grating Built into the Surface of the Model

A method which eliminates the aforementioned difficulties is based on making the grating an integral part of the test surface. The technique allows the direct measurement of the distortions from the Moiré patterns generated by the superimposition of pictures of the grating in both distorted and undistorted conditions of the model. The following conclusions are obtained:

- The technique requires an independent accurate measurement of the geometry and position of the test model in its undistorted condition. This is achieved using the same grating built into the surface of the model.

- A null method is used to measure the distortion from the images of the grating thereby eliminating the errors introduced in the fringe spacing measurements.
- The null method measures magnitude and sign of the distortions. Consequently the distortion of the test surface is uniquely defined.
- The technique provides an automatic identification of reference points on the model.
- The null method used in analyzing the images of the grating, in both distorted and undistorted conditions, can be implemented either optically or electronically in the data acquisition system.
- The technique measures a rotation in the plane of the test surface.

In conclusion, the null method, with the grating built into the model, provides the most precise measurements of the distortions, fits best the requirements and consequently is considered the most suitable technique for the anticipated instrumentation.

## 3. RECOMMENDATIONS

Based on the results of the study of the Moiré techniques developed under the present contract, the following recommendations are made regarding the instrumentation of the anticipated HIRT facility.

- Develop the instrumentation for distortion measurements on the basis of the Moiré technique with the grating built into the surface of the test model.
- Use gratings with a period of approximately .037 inches in strips .5 to 1.0 inches wide, built along the lines of the model where the measurements are planned.
- Use the null method in analyzing the Moiré patterns.
- Design the instrumentation for measurement of the geometry and position of the test model using the same grating built into the surface of the test model.
- Use two cameras for observation of the test model through two windows in the wall of the test section.
- Prior to the test run, derive the geometry and position of the model from the null method applied to two images of the grating obtained with the two cameras.
- Derive the distortion of the test model from the null method applied to the two images of one camera in both distorted and undistorted conditions of the test model.
- Use a 35 mm format for the film with cameras running at a speed of about 200 frames per second to compensate for model oscillations at frequencies up to 50 Hz.

## REFERENCES

1. Anon., Program Development Booklet for the 390-128 Transonic Aerodynamics Wind Tunnel (High Reynolds Number, HIRT), Arnold Engineering Development Center, September 1971.

2. D. M. Meadows, W. D. Johnson, J. B. Allen,"Generation of Surface Contours by Moiré Patterns," Applied Optics, Vol. 9, No. 4, pp. 942-947, April 1970.

3. H. Takasoki, "Moiré Topography," Applied Optics, Vol. 9, No. 5, pp. 1467-1472, June 1970.

4. J. B. Allen, D. M. Meadows, "Removal of Unwanted Patterns from Moiré Contour Maps by Grid Translation Techniques," Applied Optics, Vol. 10, No. 1, pp. 210-212, January 1971.

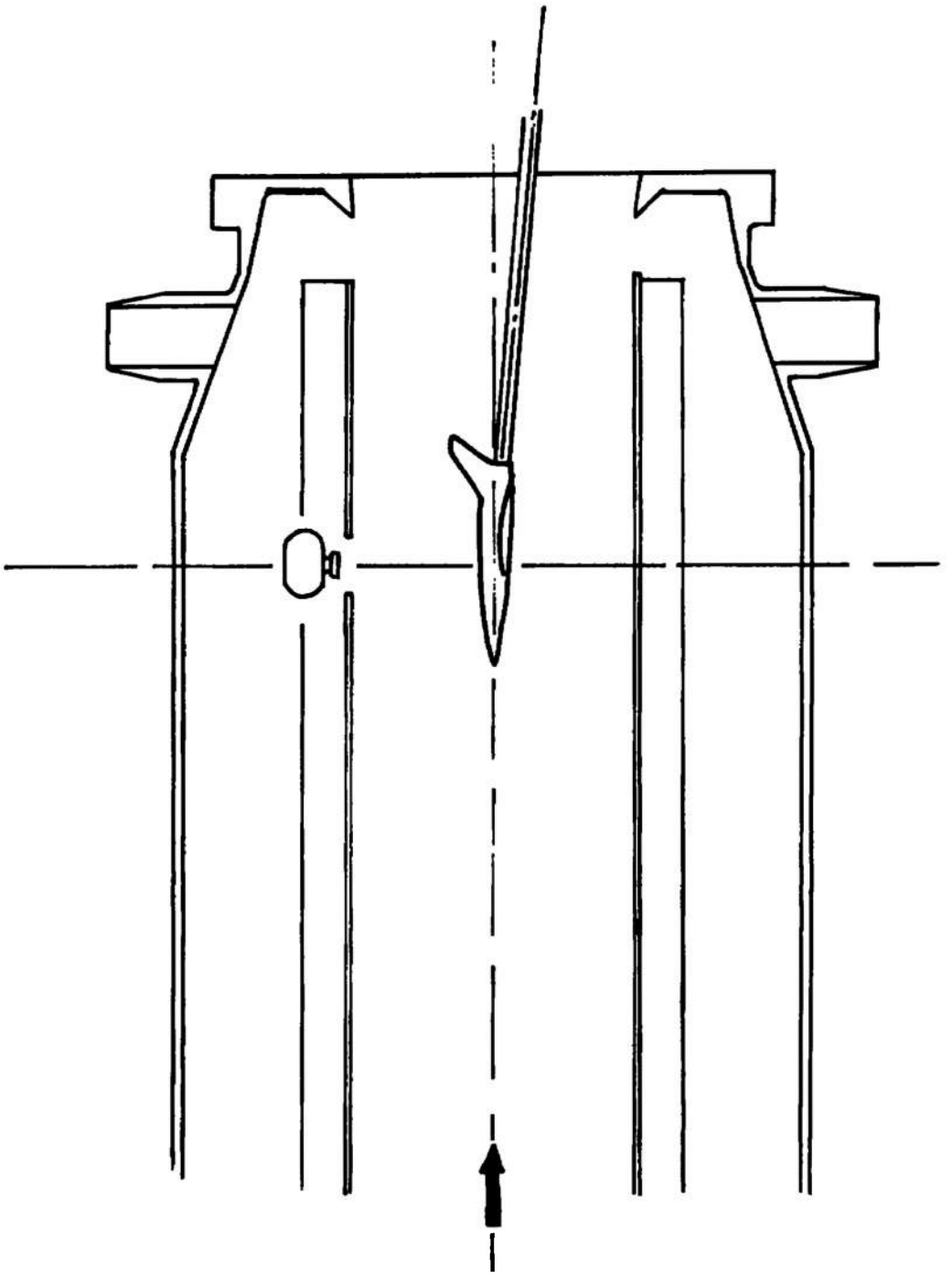

Fig. 1 Test Section of the Anticipated HIRT Facility

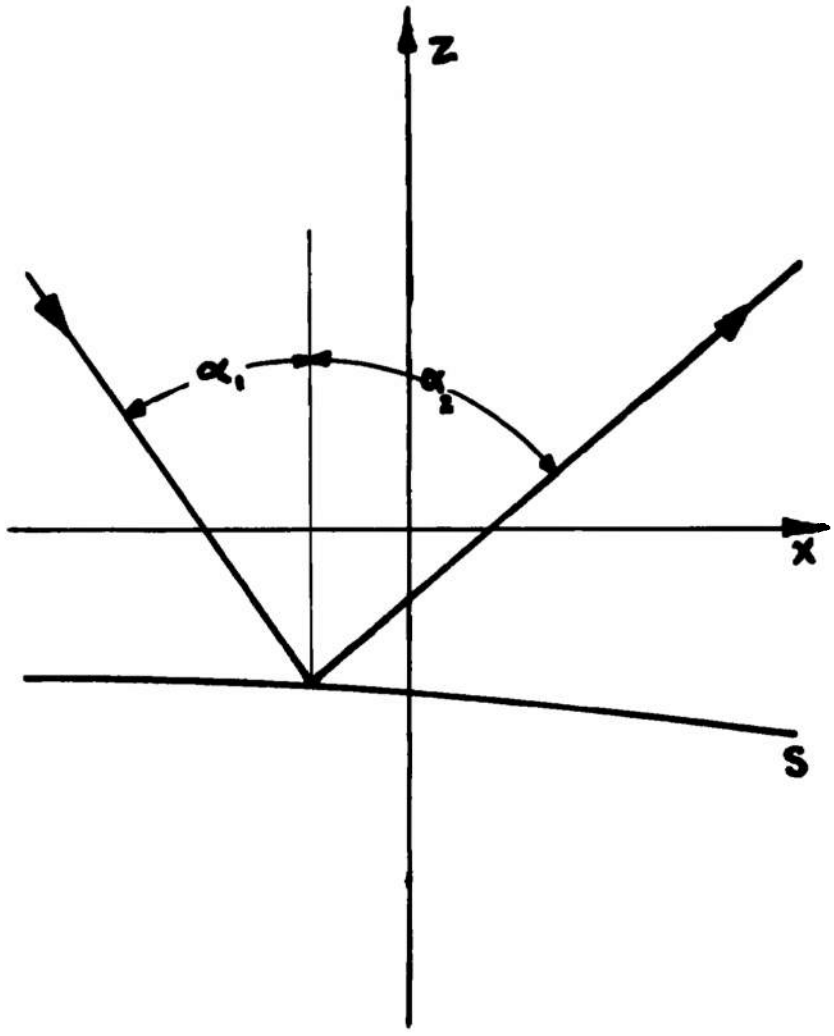


Fig. 2 Schematic of Conventional Moiré Technique

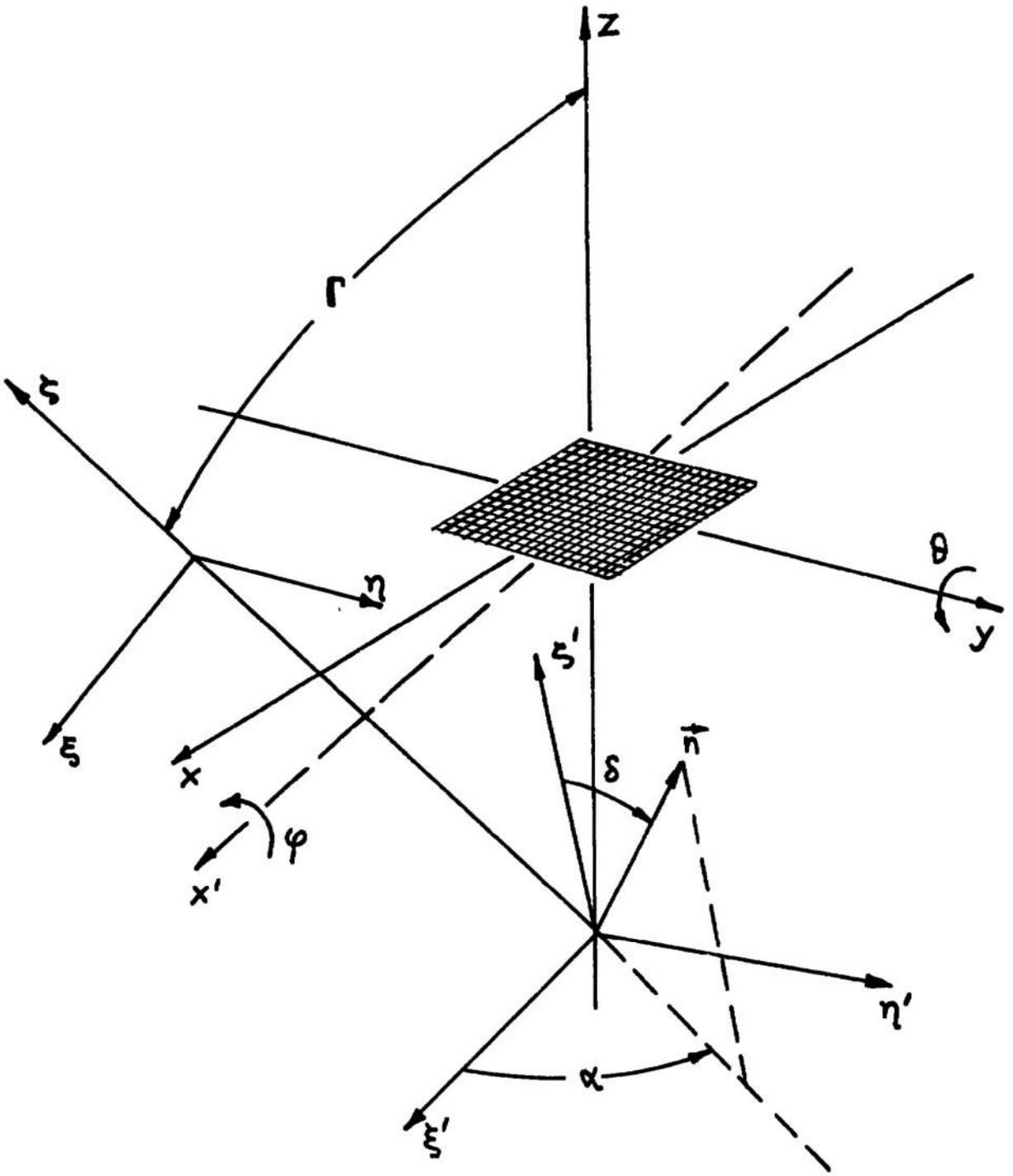


Fig. 3 Reference Systems for the Moiré Technique with a Projected Grating

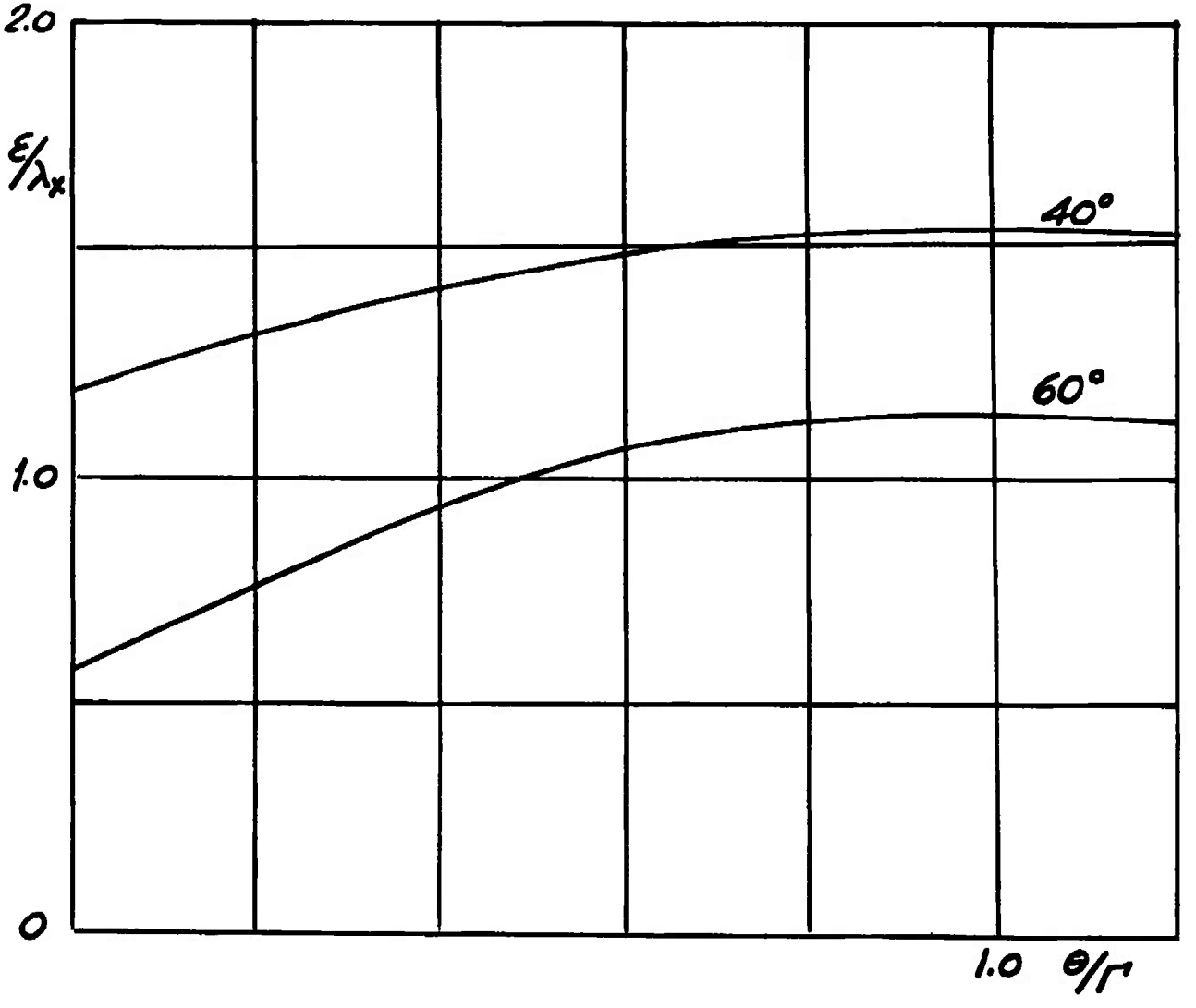


Fig. 4 Scale Factor as a Function of the Orientation of the Test Surface

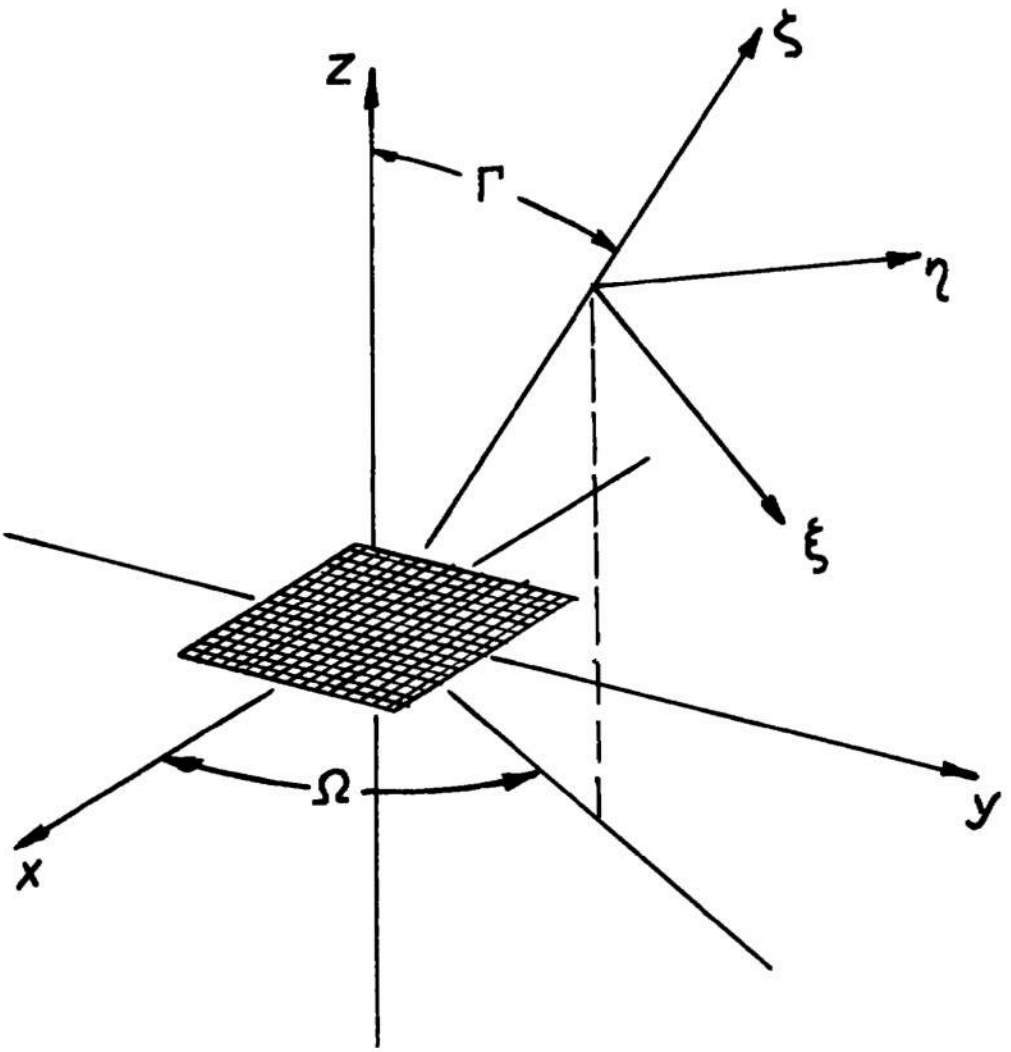


Fig. 5 Reference Systems for the Moiré Techniques with the Grating Built into the Test Surface

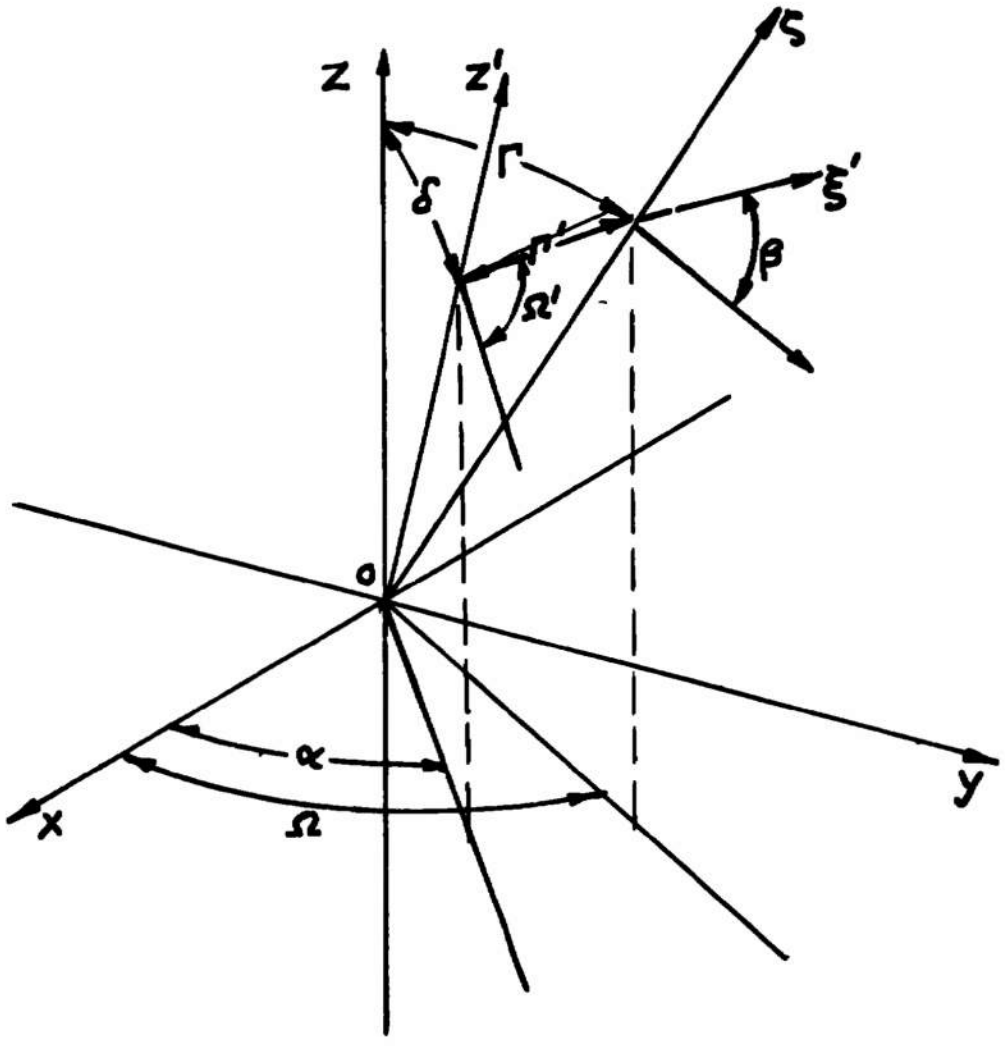


Fig. 6 Transformation of the Reference Systems to Describe the Distortion of the Test Surface

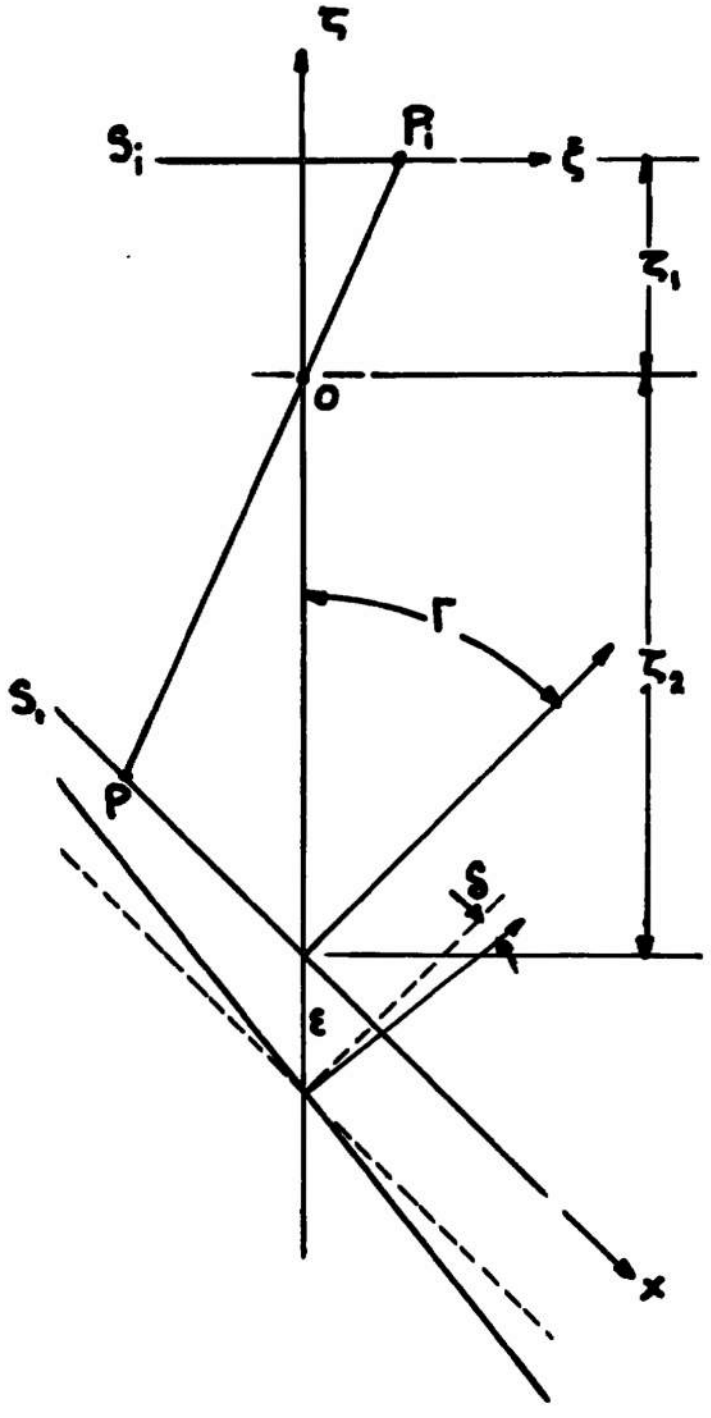


Fig. 7 Observation at a Finite Distance from the Test Surface

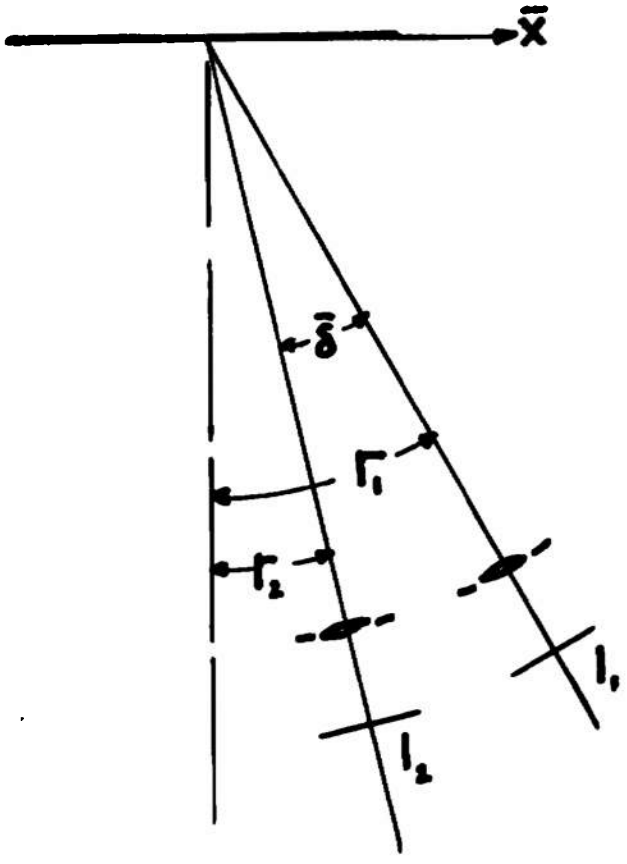


Fig. 8 Schematic of the Null Method

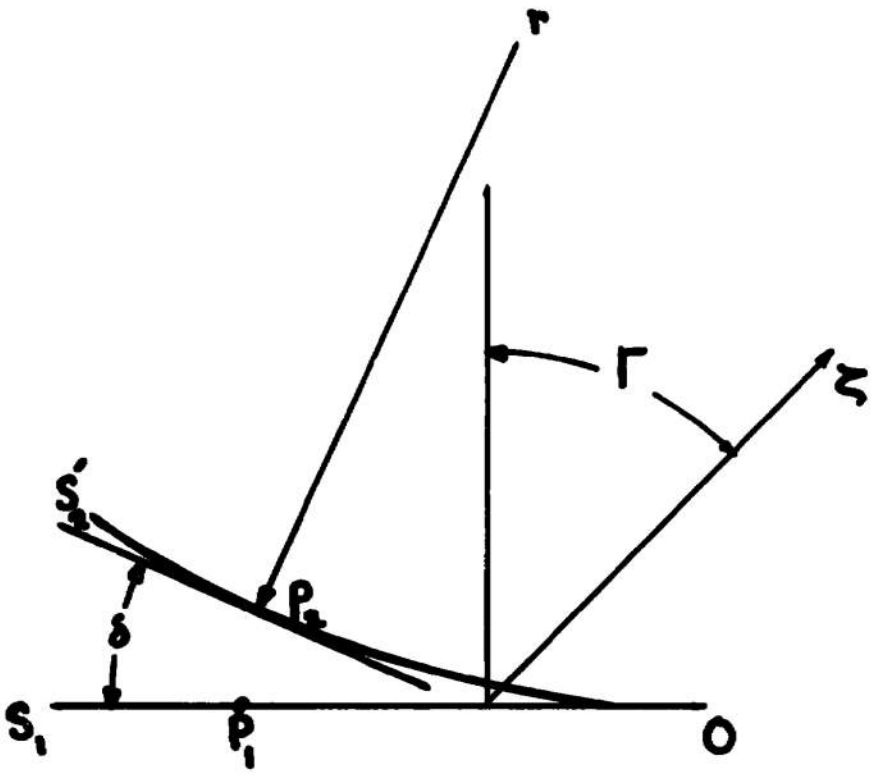


Fig. 9 Bending of the Test Surface

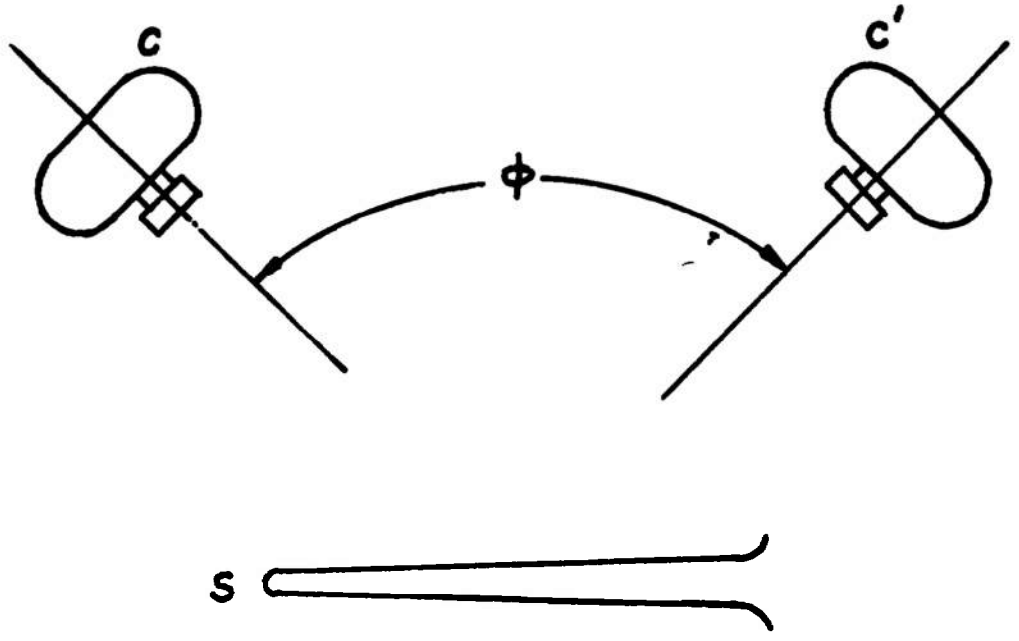


Fig. 10 Schematic of the Measurement of the Position and Geometry of the Test Surface

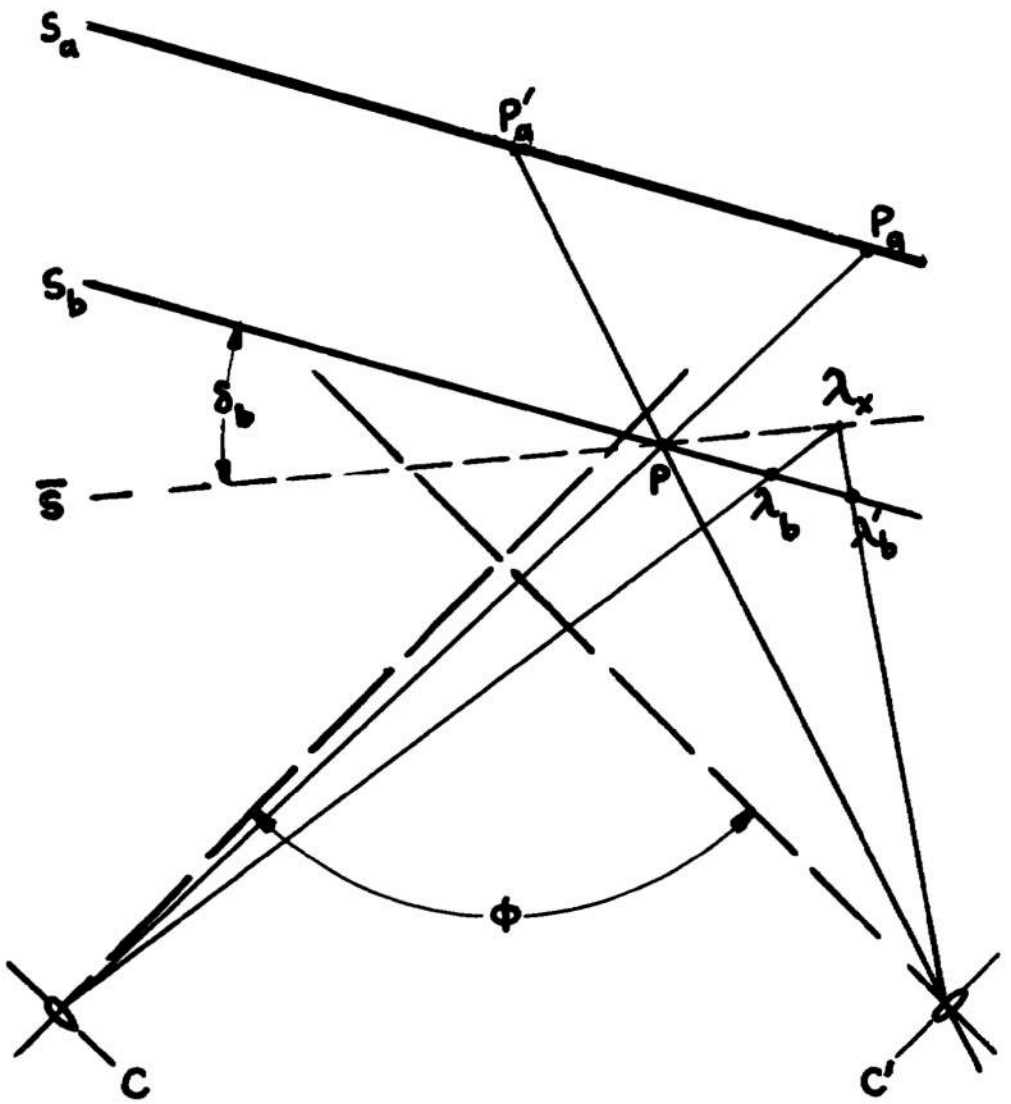


Fig. 11 Measurement of Geometry and Position

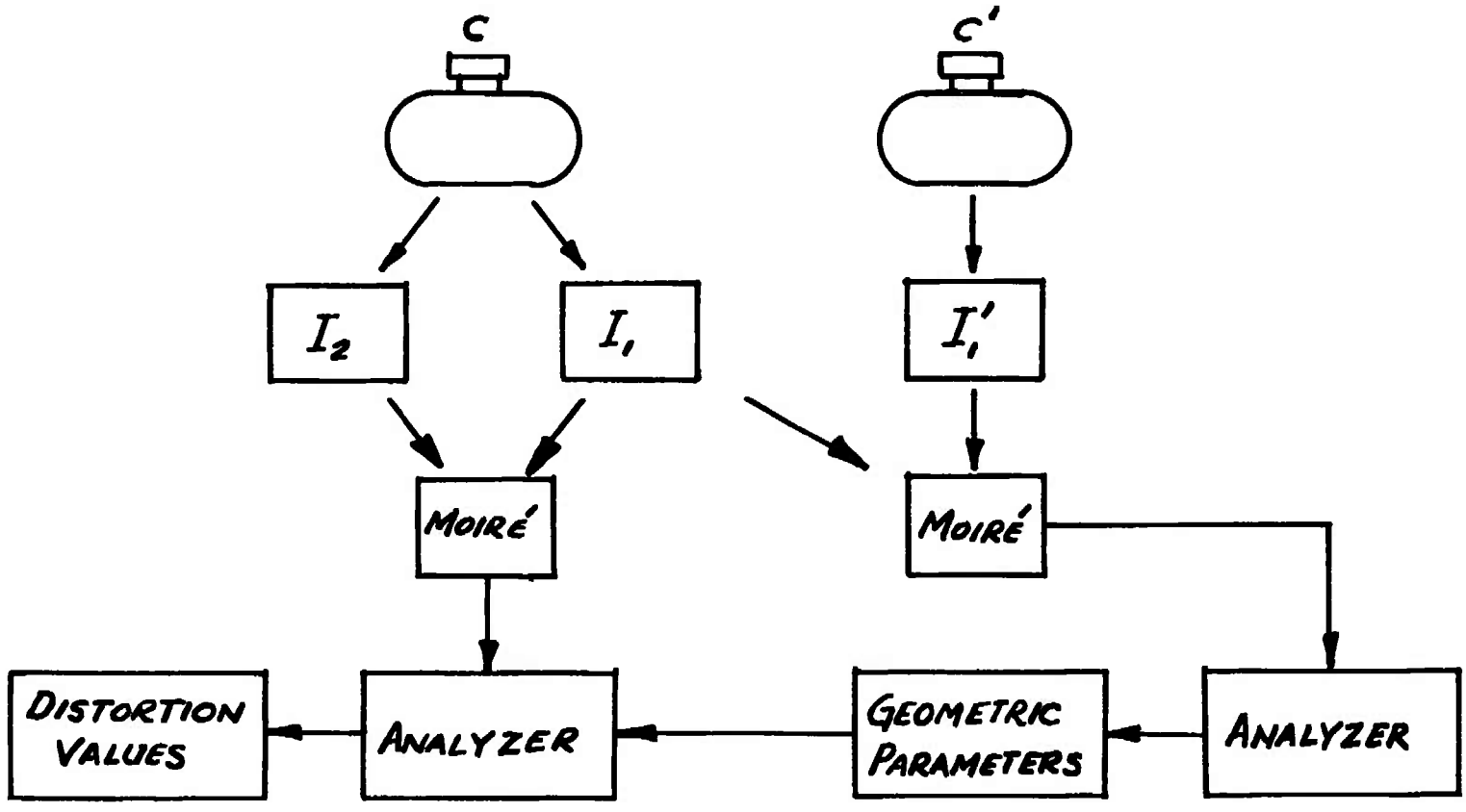


Fig. 12 Schematic of Measuring Technique

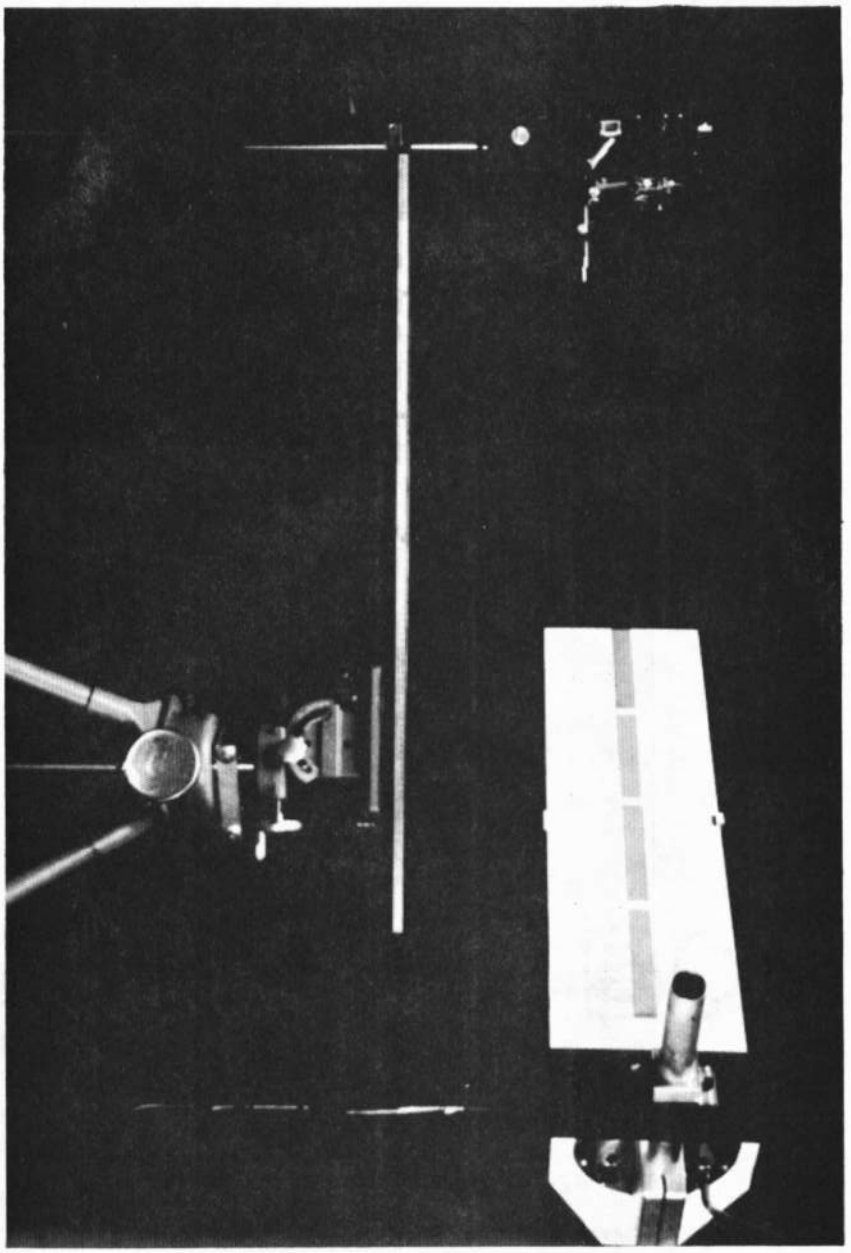

Fig. 13 Experimental Arrangement

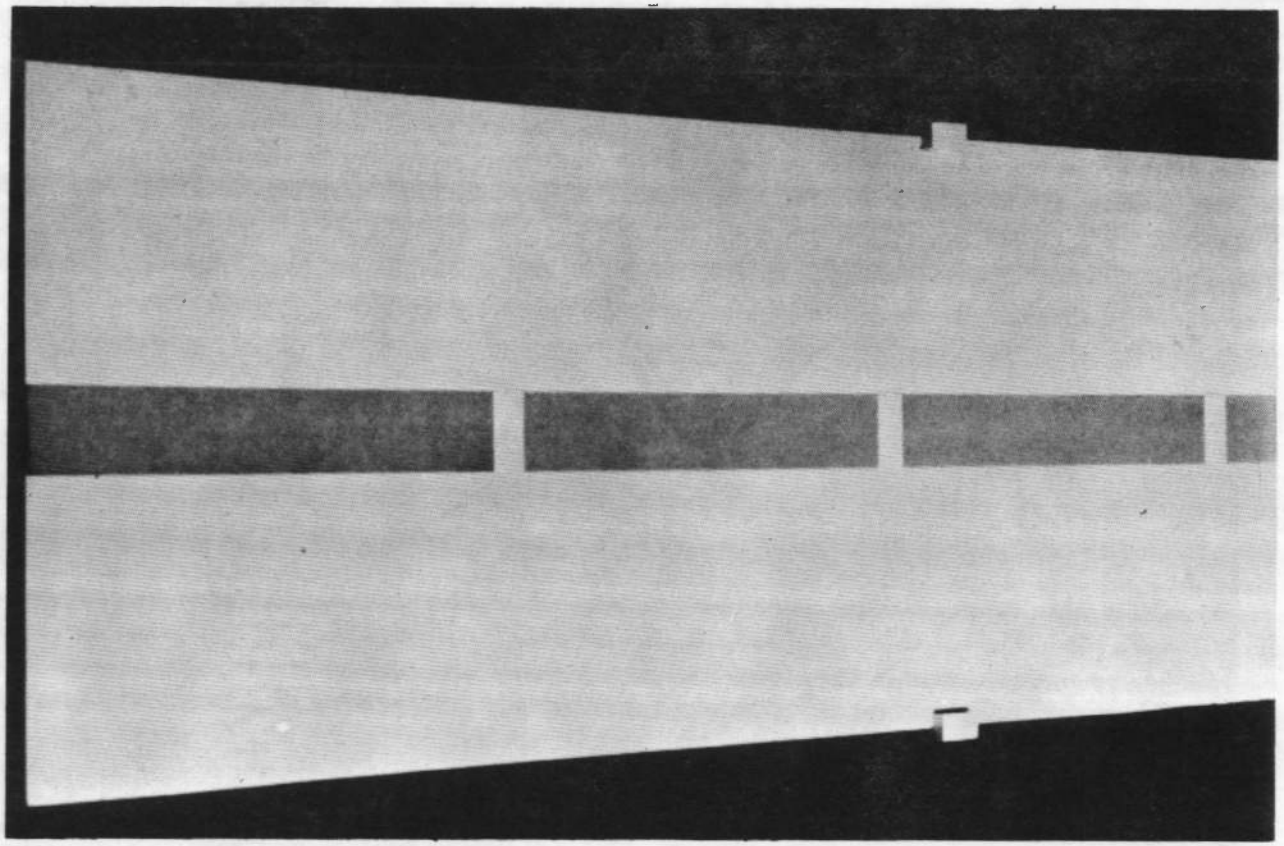

Fig. 14 Grating Applied to the Test Surface

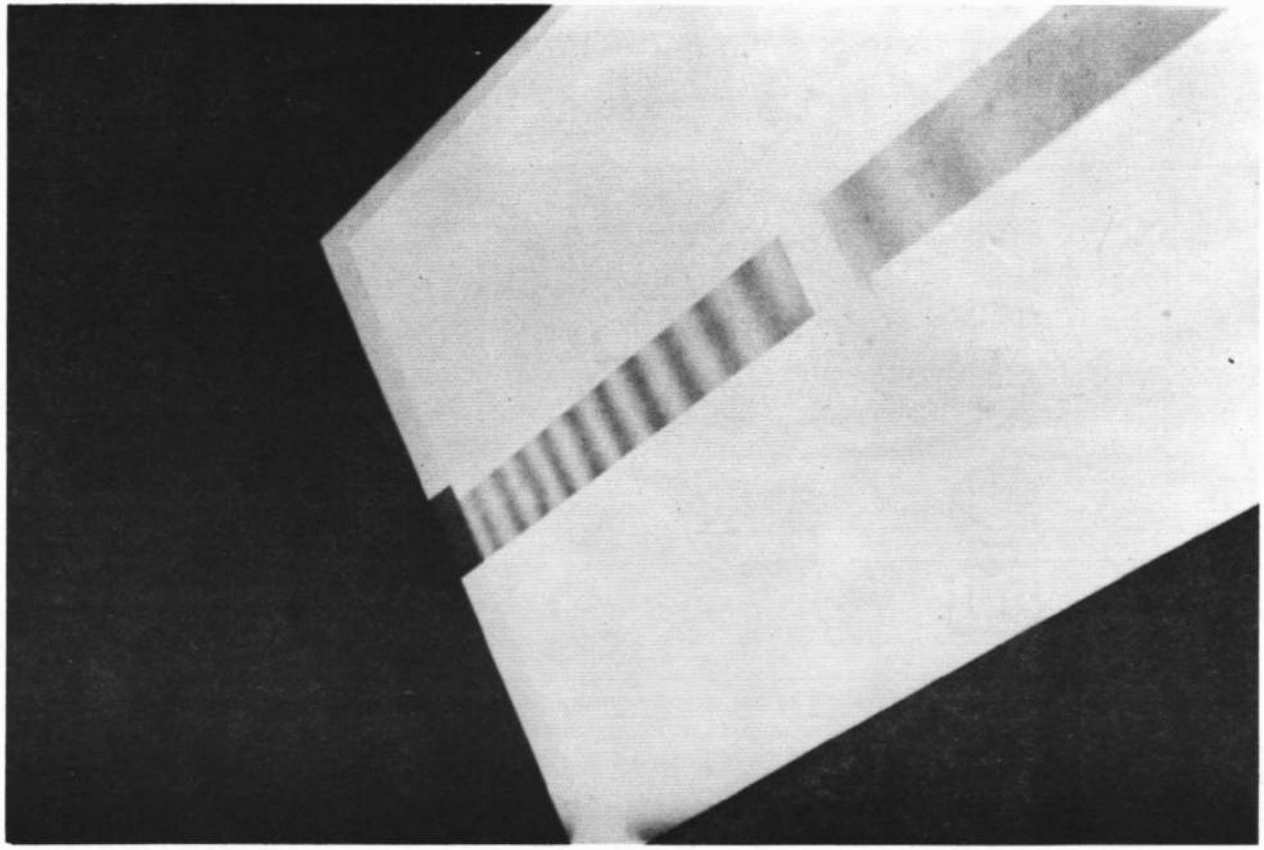

Fig. 15 Moiré Pattern

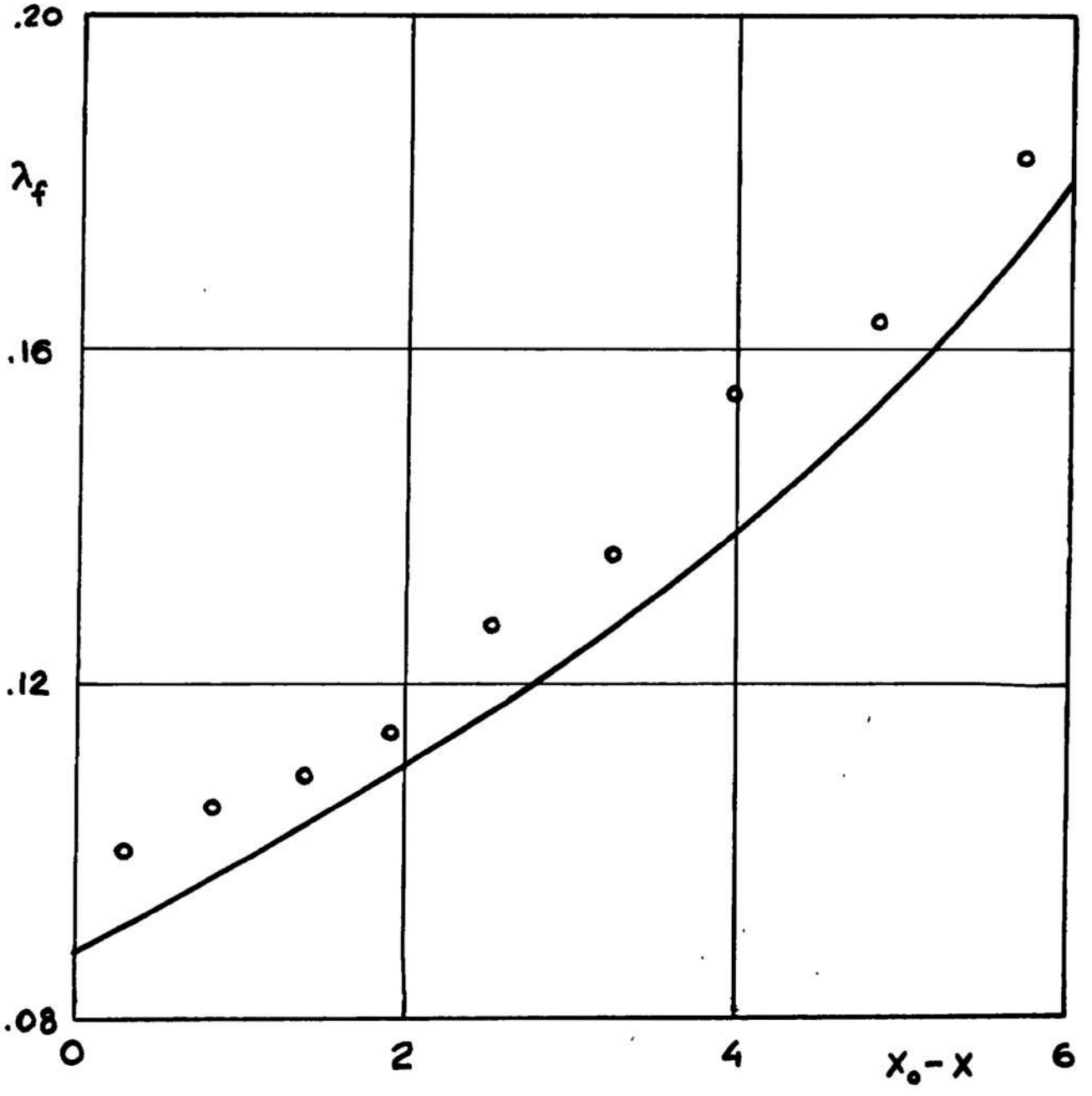


Fig. 16 Computed (Solid Line) and Experimental (Dots) Values of the Distance $\lambda_f$ Between Moiré Fringes

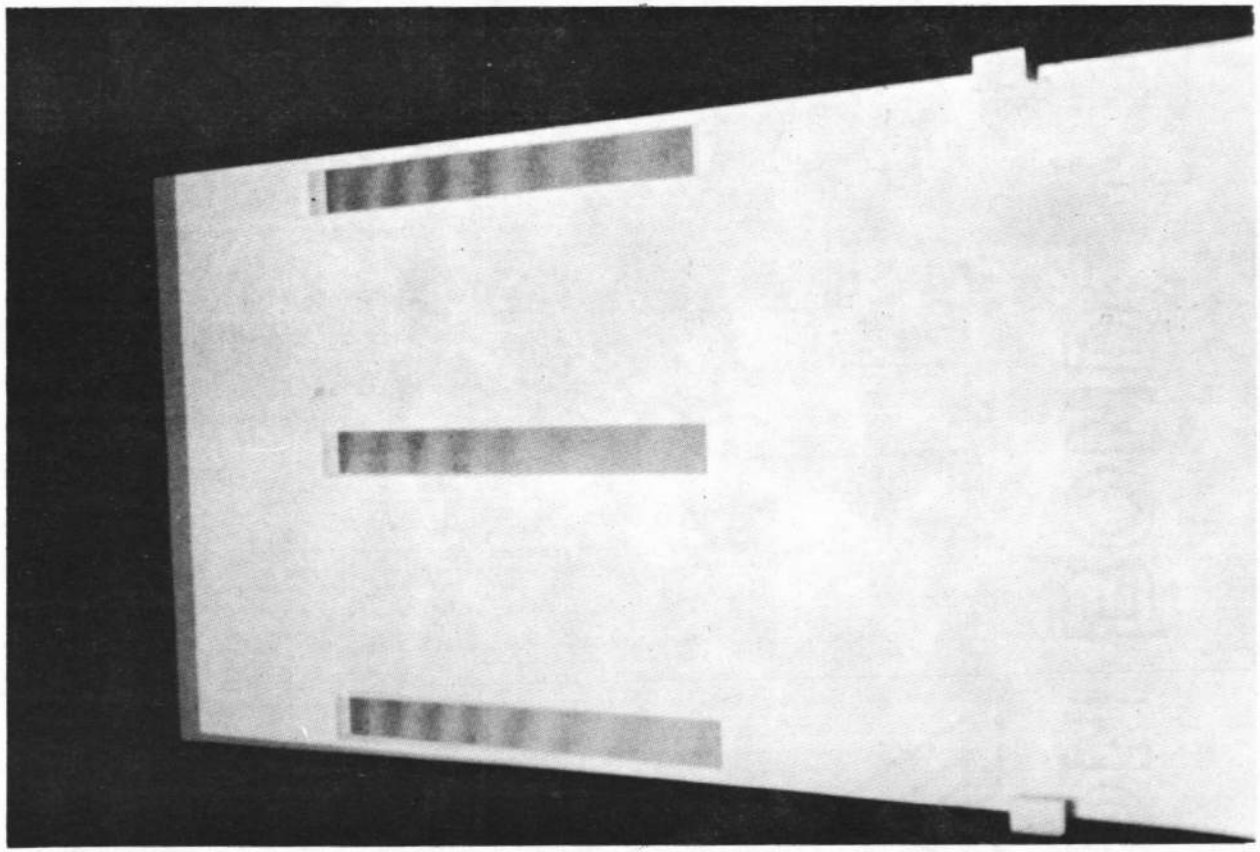

Fig. 17 Moiré Pattern for Bending of the Test Surface

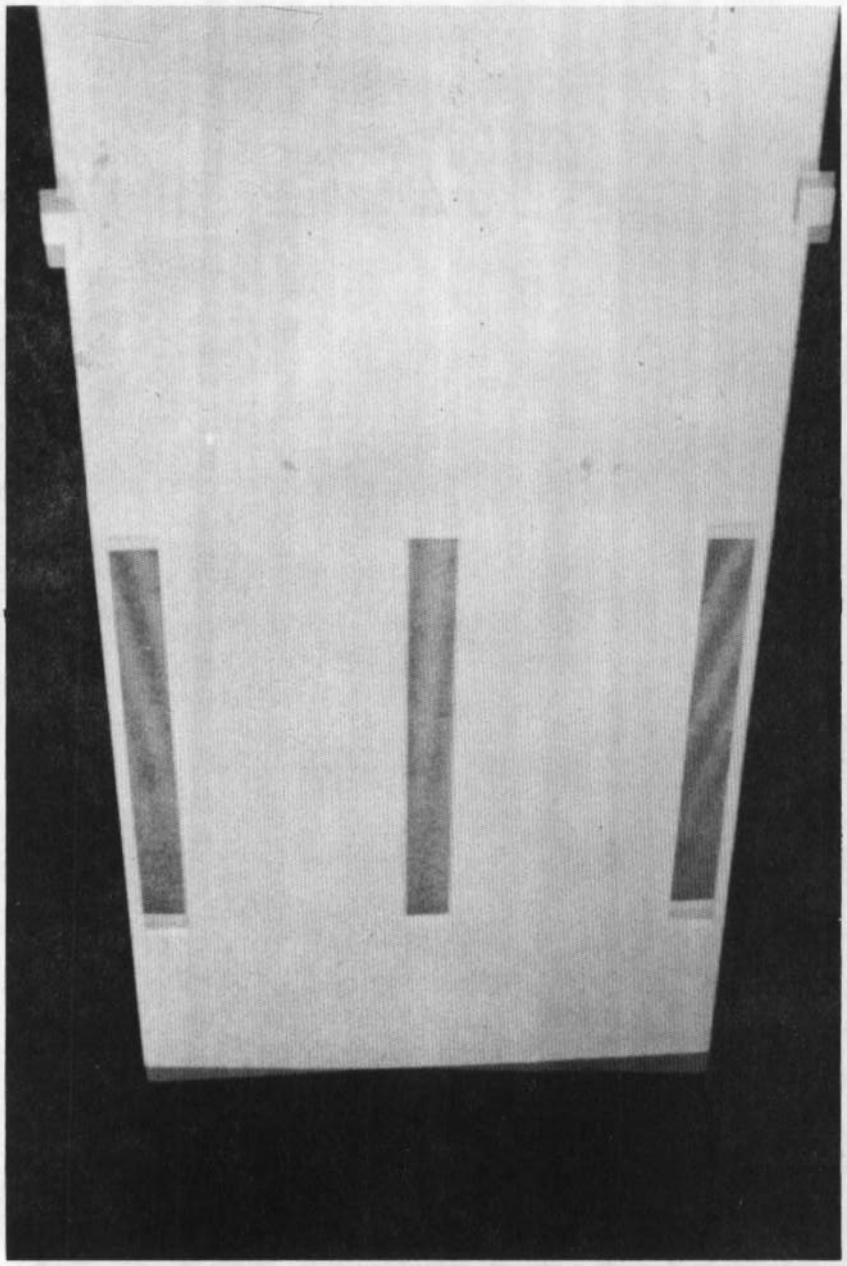

Fig. 18 Moiré Pattern for Twisting of the Test Surface

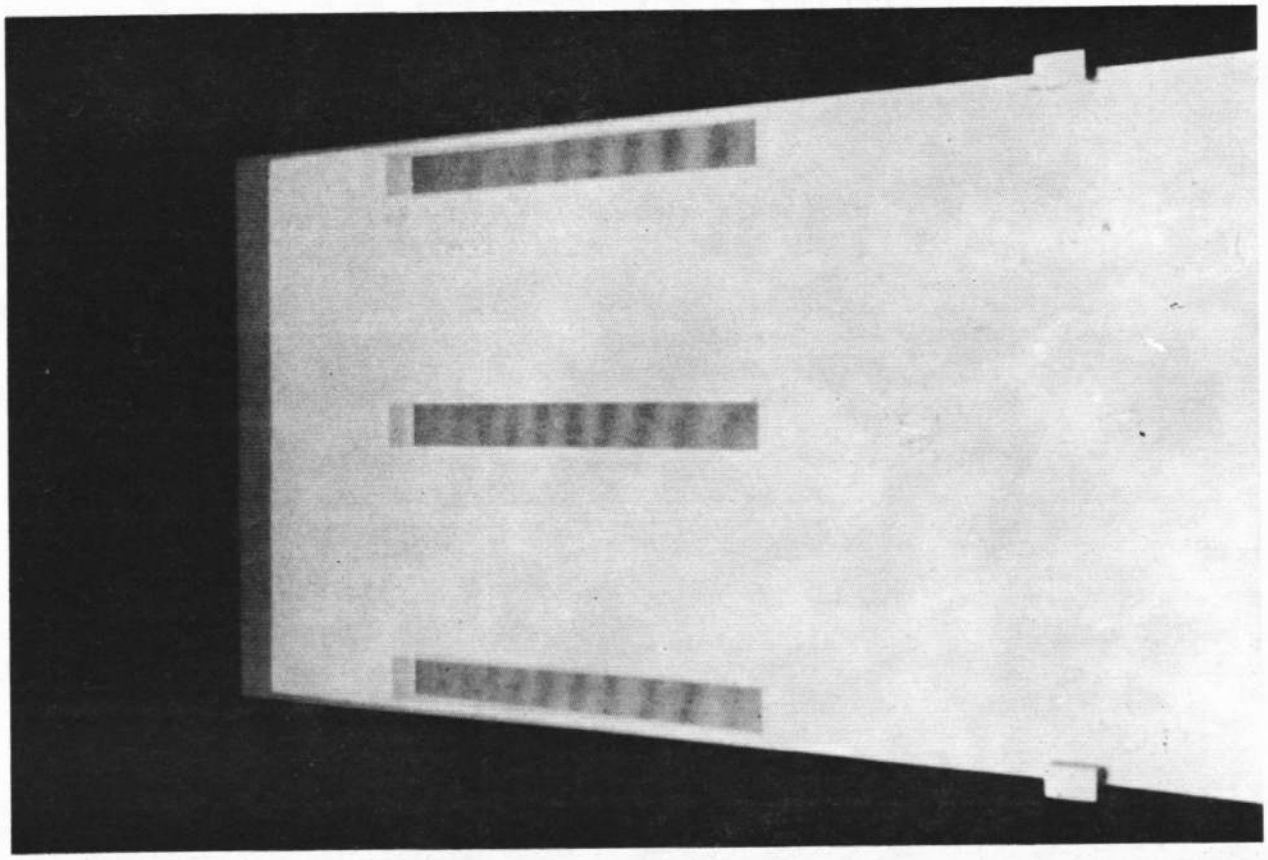

a. Moiré Pattern for Test Surface Bending

Fig. 19 Example of Null Method Procedure

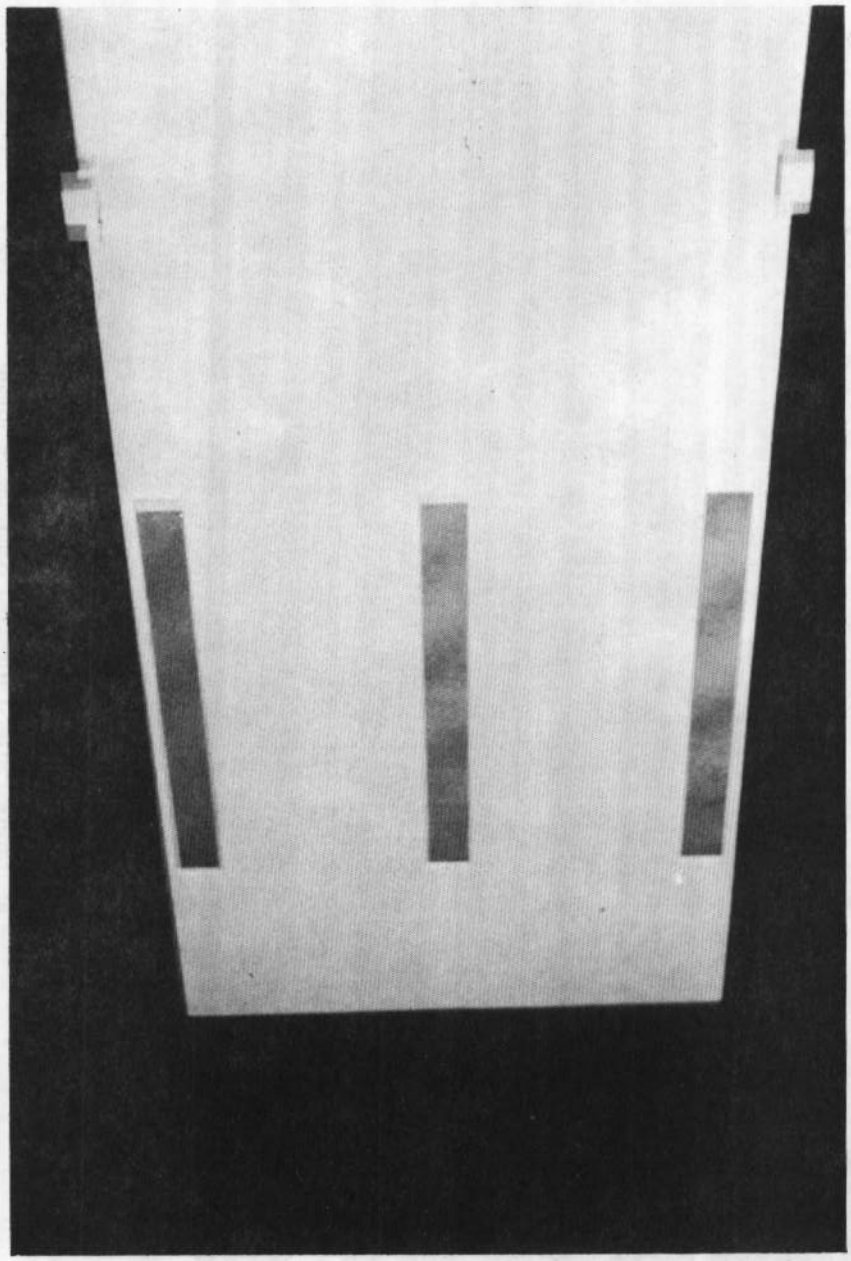

b. Partial Cancellation of the Moiré Pattern
Fig. 19 Concluded

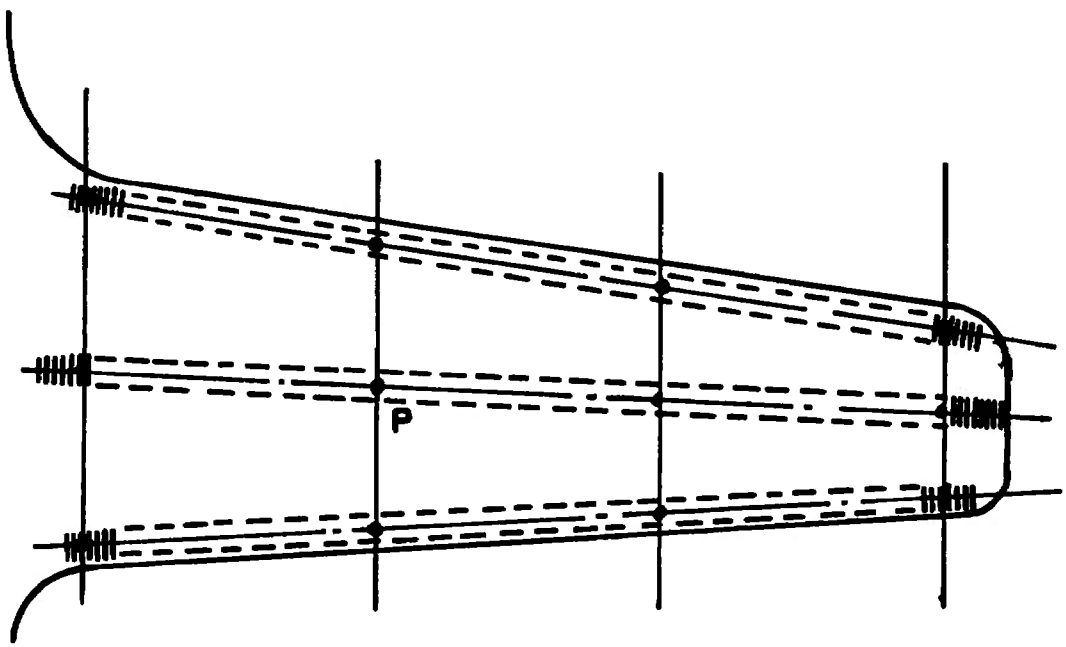


Fig. 20 Schematic of Anticipated Experimental Arrangement of the Test Model

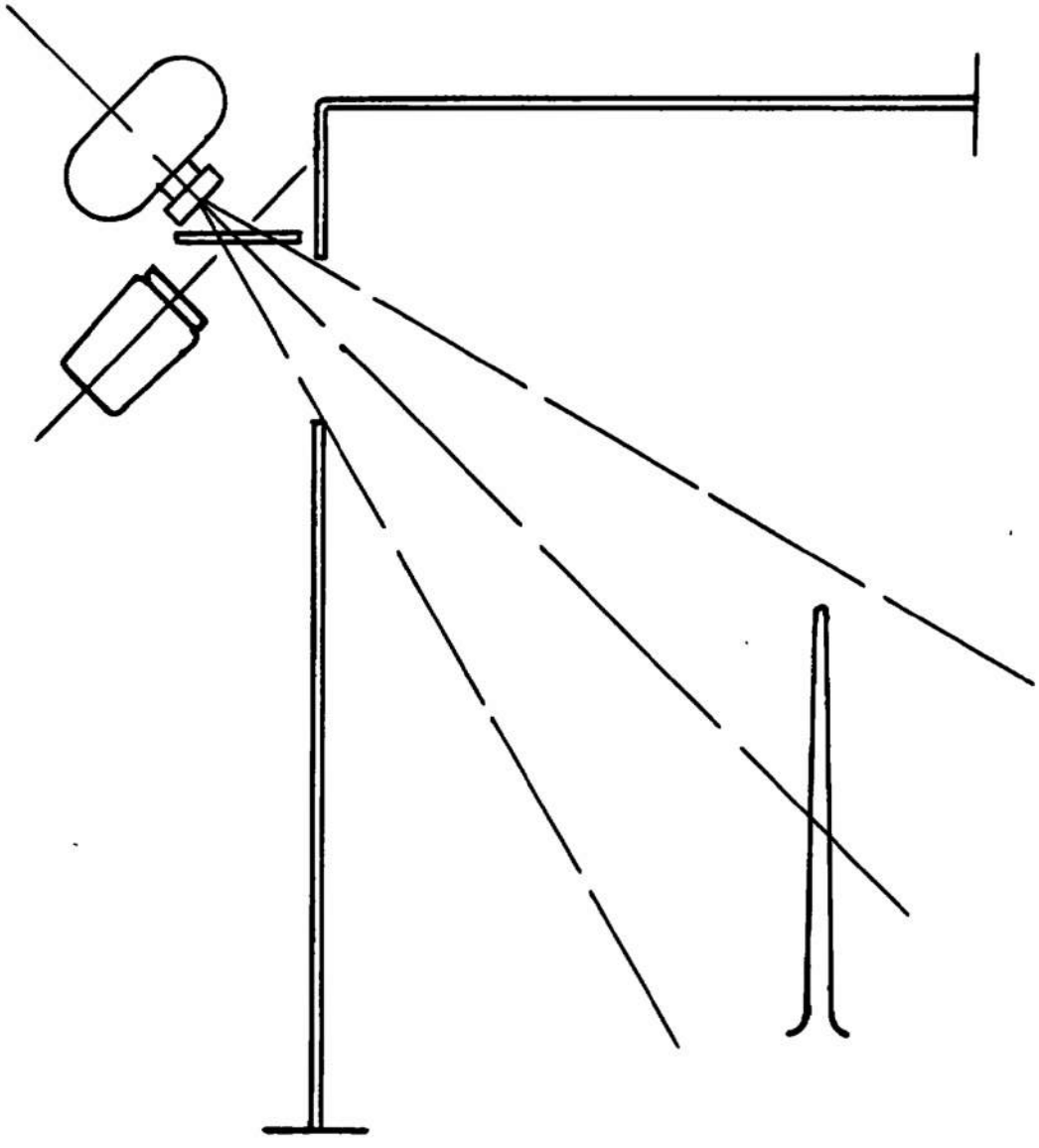

Fig. 21 Camera and Light Source Arrangement

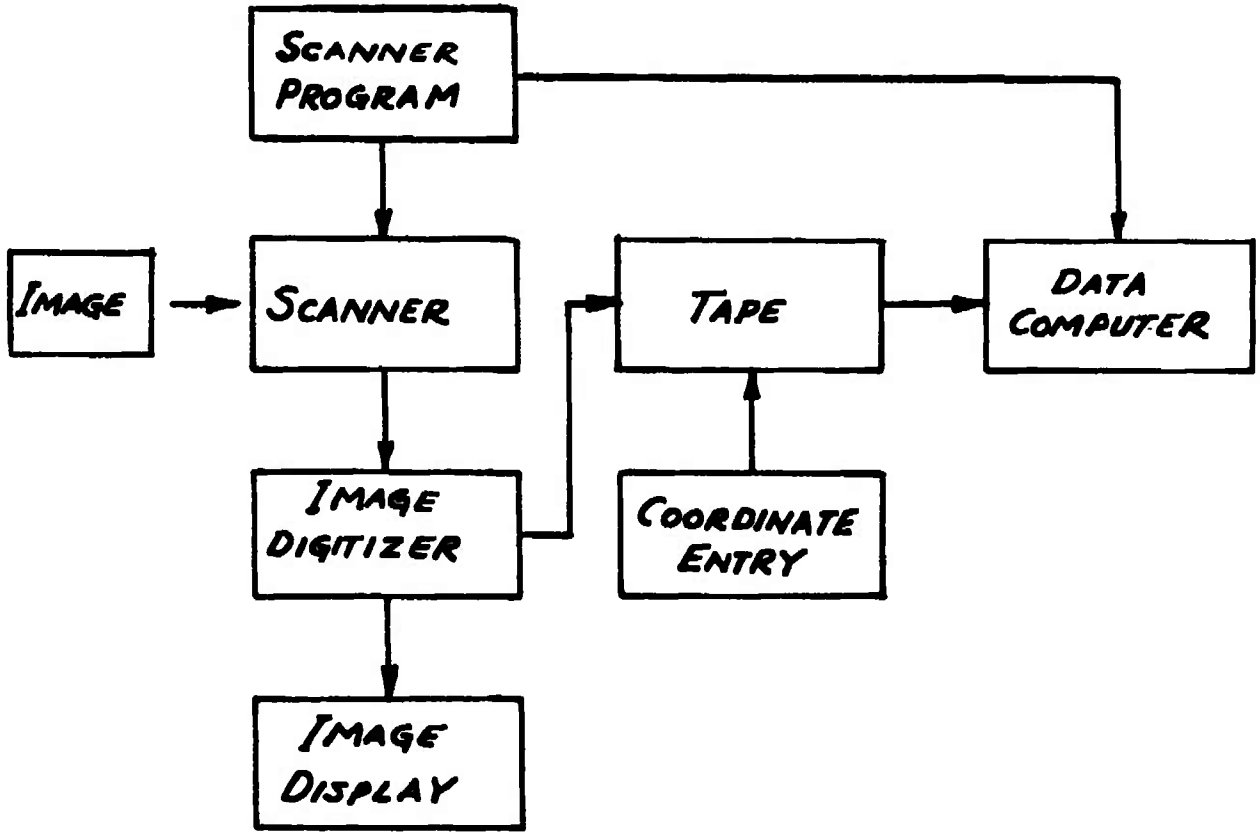


Fig. 22 Schematic of the Data Acquisition System

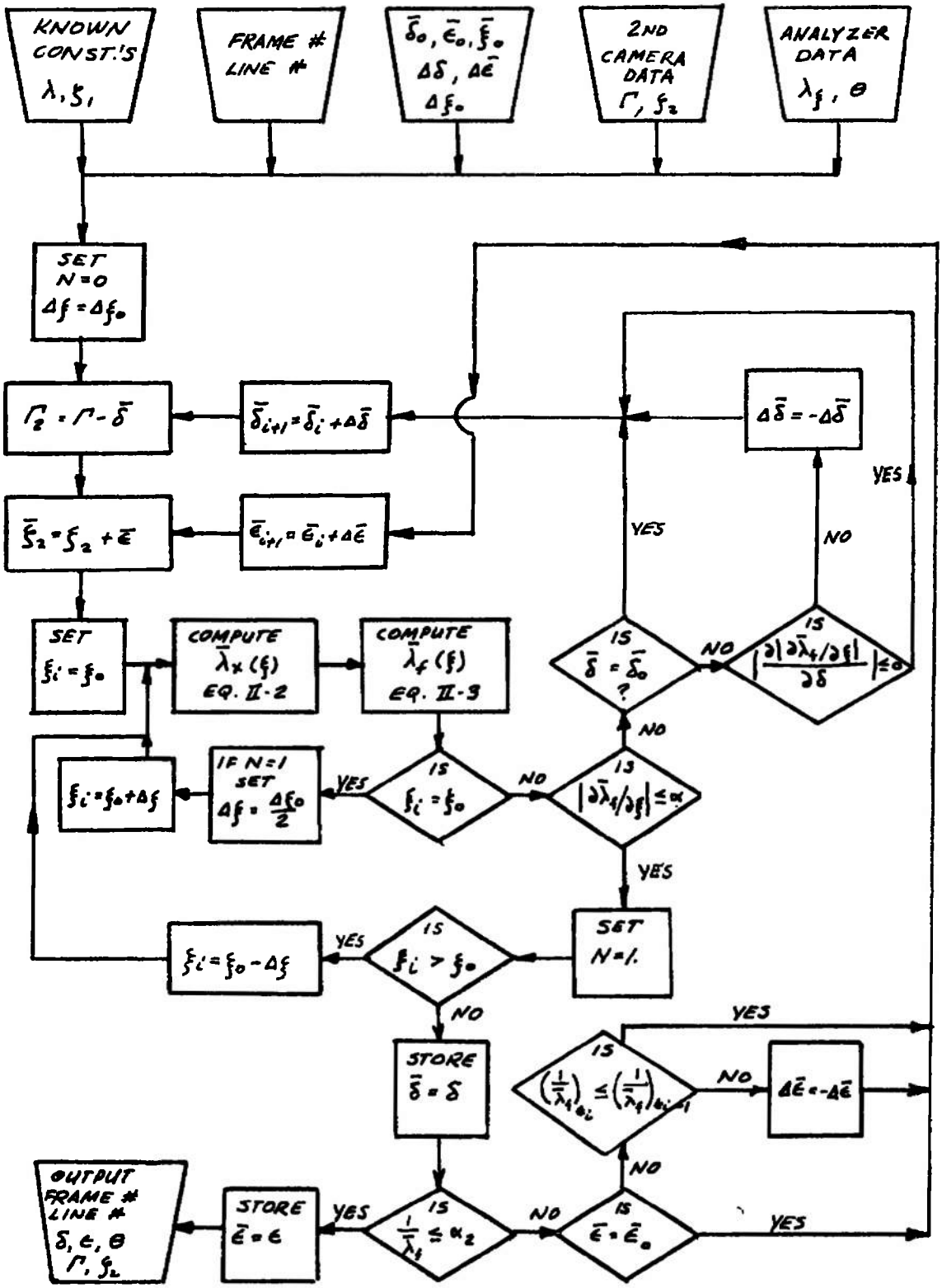


Fig. 23 Typical Data Reduction Program

UNCLASSIFIED

Security Classification

**DOCUMENT CONTROL DATA - R & D**

*(Security classification of title, body of abstract and indexing annotation must be entered when the overall report is classified)*

| 1 ORIGINATING ACTIVITY (Corporate author) | 2a. REPORT SECURITY CLASSIFICATION |
|---|---|
| Arnold Engineering Development Center<br>Arnold Air Force Station, Tennessee 37389 | UNCLASSIFIED |
| | 2b. GROUP<br>N/A |

3 REPORT TITLE

STUDY OF MOIRE MEASURING TECHNIQUES FOR WIND TUNNEL MODEL DEFORMATION

4. DESCRIPTIVE NOTES (Type of report and inclusive dates)

Final Report

5 AUTHOR(S) (First name, middle initial, last name)

Manlio Abele, Charles Ruger, and Ernest Sanlorenzo,
General Applied Science Laboratories, Inc.

| 6 REPORT DATE | 7a. TOTAL NO. OF PAGES | 7b. NO OF REFS |
|---|---|---|
| September 1973 | 70 | 4 |

| 8a. CONTRACT OR GRANT NO | 9a. ORIGINATOR'S REPORT NUMBER(S) |
|---|---|
| b. PROJECT NO | AEDC-TR-73-154 |
| c. Program Element 65802F | 9b. OTHER REPORT NO(S) (Any other numbers that may be assigned this report) |
| d. | |

10 DISTRIBUTION STATEMENT

Approved for public release; distribution unlimited.

| 11. SUPPLEMENTARY NOTES | 12. SPONSORING MILITARY ACTIVITY |
|---|---|
| Available in DDC. | Arnold Engineering Development Center, Air Force Systems Command, Arnold Air Force Station, TN 37389 |

13. ABSTRACT An analytical and experimental study has been conducted to determine the feasibility of using Moiré techniques for the accurate measurement of model distortions expected to be encountered in the HIRT Facility. A comprehensive study of the basic characteristics of Moiré techniques has been carried out to determine the best approach which could both satisfy the constraints imposed by the size and configuration of the test section, and provide the necessary accuracy in the measurement of the local distortion. The results of the study suggest the selection of a measuring technique where the grating is an integral part of the surface of the test model. A Moiré is formed by the superimposition of two images of the grating obtained in the undistorted and distorted condition of the test model. A null method of analyzing the Moiré pattern allows the accurate measurement of the local distortion. The report is presented in three parts. Part I presents a technical discussion of the measuring techniques as well as the experimental data obtained in a laboratory arrangement which simulates the anticipated test conditions. Part II discusses the implementation aspects of the recommended measuring technique. Part III contains the summary of various implementations of the Moiré principle and the recommendations regarding the selection of the most appropriate measuring technique.

DD FORM 1 NOV 68 1473

UNCLASSIFIED

Security Classification

| 14. KEY WORDS | LINK A | | LINK B | | LINK C | |
|---|---|---|---|---|---|---|
| | ROLE | WT | ROLE | WT | ROLE | WT |
| wind tunnels | | | | | | |
| Moiré effects | | | | | | |
| Moiré fringes | | | | | | |
| model distortions | | | | | | |
| high Reynolds number tunnel | | | | | | |

AFSC
Arnold AFS Tenn